ELSEVIER

Computational Materials Science 15 (1999) 196–235

COMPUTATIONAL MATERIALS SCIENCE

Alloy surfaces: segregation, reconstruction and phase transitions

G. Tréglia [a,*], B. Legrand [b], F. Ducastelle [c], A. Saúl [a], C. Gallis [d], I. Meunier [a], C. Mottet [e], A. Senhaji [f]

[a] *CRMC²-CNRS, Campus de Luminy, Case 913, 13288 Marseille Cedex 9, France*
[b] *SRMP/DECM, C.E.A. Saclay, 91191 Gif-sur-Yvette Cedex, France*
[c] *LEM, ONERA-CNRS, BP 72, 92322 Chatillon Cedex, France*
[d] *PSI, P.O. Box 513, 5600 MB Eindhoven, The Netherlands*
[e] *IRPHE-CNRS 138, Campus de St Jérôme, Service 252, 13397 Marseille Cedex 20, France*
[f] *Département de Physique, Université Mohamed I, BP 524 Oujda, Maroc*

Abstract

Surface segregation in alloys, i.e., concentration modulation in the surface selvedge at thermodynamical equilibrium, can be viewed as resulting from two kinds of competition or synergy. The first one is between surface and bulk interactions, i.e., surface energy versus bulk alloying interactions, whereas the second one is between these chemical forces and the atomic size-mismatch. Modelling the phenomenon then requires to account for all these forces on the same level. This leads to use both realistic energetic models derived from electronic structure and efficient statistical tools, from mean–field approximation to Monte Carlo simulations. A particular attention must be payed to the possible multisolution character of the problem. Actually, the possible coexistence of stable and metastable solutions may be at the origin of superficial phase transitions, in which the surface acts as a precursor of bulk order–disorder transitions: layering transitions, concentration profile transitions, surface induced order or disorder. All these phenomena are illustrated here on some specific systems and analyzed with tools derived from tight-binding formalism. Finally, the strong coupling between surface segregation and atomic reconstructions is illustrated in the case of strong size-mismatch by means of molecular dynamics calculations.

Keywords: Surface segregation; Phase transition; Superstructure

1. Introduction

From a semantic point of view, surface segregation refers to the variation of the composition in the surface selvedge of an alloy at thermodynamical equilibrium [1]. Let us emphasize that one has to be careful not to confuse this segregation phenomenon which is an equilibrium state in a single phase region of the bulk phase diagram, with processes occurring in two-phases bulk states which can be of either kinetical nature (preferential precipitation) or equilibrium one (choice of the surface phase, in which a possible

* Corresponding author. Tel.: +33 4 91 17 28 85; fax: +33 4 91 41 89 16; e-mail: treglia@crmc2.univ-mrs.fr

0927-0256/99/$ – see front matter
PII: S0927-0256(99)00004-X

single-phase segregation may still takes place) [2]. Studying this phenomenon, either experimentally or theoretically, requires to answer the following questions.

1. What is the nature of the segregating element?
2. How does the surface concentration vary as a function of bulk concentration for a given temperature? This defines the segregation isotherm. Moreover what is the influence of temperature and surface crystallographic orientation on this segregation isotherm?
3. How far does extend the perturbation due to the surface? This defines the concentration profile.
4. What is the nature of this profile (oscillating or monotonous)?
5. How does the concentration vary, in a given plane parallel to the surface for sites which are inequivalent, either from the crystallographic point of view, in presence of reconstruction, or from the chemical one in case of two-dimensional ordering or phase separation?

Most of the theoretical work has been devoted to the prediction of the existence (or not) of such a surface enrichment and of the nature of the segregating species [3]. From these studies, it has been possible to draw the main three driving forces of the phenomenon, namely the differences in surface energy and size between the components and their ability to mix or not in the bulk (mixing energy) [4]. Moreover, the latter term has been identified as responsible of the nature of the concentration profile [5,6]. Most of these studies have been performed for disordered alloys (i.e., for temperatures higher than the critical ones between disorder and order or phase separation: $T > T_c$). However, it has been shown also that at lower temperature ($T < T_c$) bulk ordering effects could compete with these surface driving forces on one hand [7], and that surface could act as a precursor for bulk ordering [8], bulk disorder [9] or phase separation phenomena [10], or even lead to specific ordered structures [11] on the other hand. The calculations involve statistical models which have to be grounded on energetic ones. In most cases, the latter involve some empirical parameters, whose variation at the surface can drastically modify the observed behaviours [12]. It is then essential to go beyond such empirical models, for instance by grounding them on electronic structure. We will show in the following the modern ways to do that. Anyway, it is worth noticing that the level of details expected from these analysis strongly depends on the accuracy of the available tools for experimental investigation. Therefore, the requirement level has widely evolved in the recent years with the huge development of more and more sensitive surface techniques.

From this experimental point of view, many techniques have been developed in order to answer the questions raised above, at different scales depending on their sensitivity to the surface (atomic scale, or average information on a few layers) [13]. Among these techniques one finds the usual photoelectron spectroscopies such as Auger (AES) [14,15] or photoemission (ESCA, XPS-UPS, XPD) [16,17], diffraction techniques involving either electrons (LEED) [18,19] or ions (ISS, LEIS, MEIS, RBS) [20,21] or X-rays (SXRD) [22], field ion microscopy (ToF-FIM) [23,24], and even now STM imaging [25,26]. Let us note that the most widely used techniques for surface segregation studies are probably AES [14,15] and ISS [20,21]. The former only gives a mean value of the surface enrichment averaged on a few layers below the surface, while the latter, depending on the ion energies, characterizes the concentration in the surface layer only (LEIS) or on the contrary in its deep selvedge (RBS) [27]. Therefore, none of these techniques gives any information on the concentration profile. In fact, determining the latter is possible either directly by using ToF-FIM, which allows to obtain a layer by layer profile [24], or more indirectly by quantitative LEED [19] or SXRD analysis [22].

Depending on the extension of the experimental probe, one will then be able to answer one or several of the questions raised above, in particular concerning the temperature influence on surface segregation and on the nature of the concentration profile. Thus, it is tempting to determine a possible link between segregation in the disordered state and the termination of an ordered bulk compound (or more generally the concentration profile in the ordered state) [3]. Finally, a main problem which has to be addressed is the coupling between segregation and the crystallographic and morphological structure of the surface. This is related to phenomena such as the relaxation and rumpling of compound surfaces [28], the existence of

reconstructions (or superstructures) induced by the segregation process, in particular when the surface of one component is reconstructed and not the other [29–31], or finally the influence and the nature (single or double) of steps [32].

In order to illustrate all these points, the present review is organized as follows. First, we will detail the energetic (Section 2) and statistical (Section 3) models. Then we will discuss the main trends observed in solid solutions (Section 4) and in ordered compounds (Section 5). Finally, the possible coupling between surface reconstructions and segregation is debated (Section 6).

2. Energetic models

2.1. Impurity on a rigid lattice

The segregation energy, ΔE^{seg}, is defined as the energy balance involved when one atom of a given species, initially placed in the bulk, is exchanged with an atom of the other species located in the surface plane. The calculation of ΔE^{seg} in a concentrated alloy is complicated by its concentration dependence. Hence, the great deal of calculations devoted to the evaluation of this energy for a single impurity. This has been achieved using various energetic models, from empirical pairwise interactions up to electronic structure calculations at zero temperature [33–38]. Up to very recently these calculations were performed on a rigid lattice without any atomic relaxations.

2.1.1. Empirical pairwise interactions

The most simple model is based on a description of the total energy in terms of a sum of pair interactions [5]. This is the so-called Ising model which writes, for a multicomponent alloy

$$E_{\mathrm{tot}} = \frac{1}{2}\sum_{\substack{n,m\neq n\\ i,j}} p_n^i p_m^j \varepsilon_{nm}^{ij}, \tag{1}$$

where the sites are labelled by the indices n, m and the chemical species by i and j. The chemical configuration is given by the set of occupation numbers $\{p_n^i\}$, where $p_n^i = 1$ if site n is occupied by an atom of type i, and 0 if not. ε_{nm}^{ij} is the pair interaction between atom i at site n and atom j at site m. In the case of a binary alloy A_cB_{1-c}, Eq. (1) can be simplified since $p_n^{\mathrm{A}} = p_n$ and $p_n^{\mathrm{B}} = 1 - p_n$:

$$E_{\mathrm{tot}} = E_0 + \sum_n p_n \sum_{m\neq n} (\tau_{nm} - V_{nm}) + \sum_{n,m\neq n} p_n p_m V_{nm} \tag{2}$$

in which

$$E_0 = \frac{1}{2}\sum_{n,m\neq n} \varepsilon_{nm}^{\mathrm{BB}}, \quad \tau_{nm} = \frac{1}{2}(\varepsilon_{nm}^{\mathrm{AA}} - \varepsilon_{nm}^{\mathrm{BB}}) \quad \text{and} \quad V_{nm} = \frac{1}{2}(\varepsilon_{nm}^{\mathrm{AA}} + \varepsilon_{nm}^{\mathrm{BB}} - 2\varepsilon_{nm}^{\mathrm{AB}}).$$

Let us note that the second term is related to the difference in cohesive energies between A and B pure metals, while the third one gives the tendency of the system to form homoatomic ($V_{nm} < 0$) or heteroatomic ($V_{nm} > 0$) bonds between neighbouring atoms at distance R ($R = |n - m|$). In the case of interactions limited to first neighbours on a rigid lattice, and if one assumes that the interactions do not depend on the nature of the sites n and m (bulk, surface), $\tau_{nm} = \tau$ and $V_{nm} = V$, Eq. (2) can then be yet simplified into

$$E_{\mathrm{tot}} = E_0 + (\tau - V)\sum_n p_n Z_n + V \sum_{n,m\neq n} p_n p_m \tag{3}$$

in which Z_n is the number of first neighbours of site n ($Z_n = Z + 2Z'$ in the bulk and $Z_n = Z + Z'$ for a close-packed surface, in which Z and Z' are the numbers of neighbours, respectively in the same plane and in the adjacent one). Within this model, the segregation of a single A impurity to the surface of a B metal is given by the energy balance involved when exchanging a A atom in the B bulk with a B surface atom:

$$\Delta E^{\mathrm{seg}}_{\mathrm{chem}} = Z'(\varepsilon^{\mathrm{BB}} - \varepsilon^{\mathrm{AB}}) = -Z'(\tau - V). \tag{4}$$

Grouping together the interactions leads to the second expression exhibited in Eq. (4) which illustrates the role of two of main driving forces for surface segregation, namely the difference in surface energies between pure A and B elements, $\tau_{\mathrm{A}} - \tau_{\mathrm{B}} = -Z'\tau$, and the tendency of the system to order ($V > 0$) or to phase separate ($V < 0$). As can be seen, the A impurity tends to segregate ($\Delta E^{\mathrm{seg}}_{\mathrm{chem}} < 0$) if it has the lowest surface energy ($\tau > 0$), or, in absence of this first effect, for phase separating systems ($V < 0$). However, let us add that this way to rewrite Eq. (4) is just a trick in order to exhibit these driving forces, since it involves AA interactions eventhough only one atom is present!

2.1.2. Electronic structure models

In the case of a single impurity (dilute system) it is possible to go beyond empirical calculations and to calculate the corresponding segregation energy directly from the electronic structure. This can be done at various levels of approximation, from exact ab initio methods [38] to more approximate ones derived from either the jellium model for normal metals [34] or tight-binding scheme for transition metals [33,35–37]. Let us note that, up to now, most of these calculations have been performed on a rigid lattice, the relaxation effects being neglected. Since the present review is essentially devoted to transition metallic alloys, which represent most of the materials of interest for industrial applications (metallurgy, magnetism, catalysis), we will here only present results of calculations performed in the framework of the tight-binding model. In fact, even within such simplified approaches, the problem is not so simple as it seems, since one has to deal with the questions of charge transfers and self-consistency which exist also for concentrated alloys [33].

The tight-binding hamiltonian for a A impurity at site n_0 of a B matrix can be written in the basis of atomic orbitals λ at site n $|n,\lambda\rangle$:

$$\begin{aligned} H &= H_0 + V \\ H_0 &= \sum_{n,m,\lambda,\mu} |n,\lambda\rangle \beta_{nm}(\lambda,\mu) \langle m,\mu| \\ V &= \sum_{\lambda} \left\{ |n_0,\lambda\rangle (\varepsilon^{\mathrm{A}}(\lambda) + \alpha^{\mathrm{A}}(\lambda)) \langle n_0,\lambda| + \sum_{n \neq n_0} |n,\lambda\rangle (\varepsilon^{\mathrm{B}}(\lambda) + \alpha^{\mathrm{B}}(\lambda)) \langle n,\lambda| \right\} \end{aligned} \tag{5}$$

in which V accounts for the diagonal (on-site) part involving the atomic level $\varepsilon^i(\lambda)$ and crystal field $\alpha^i(\lambda)$, for $i = \mathrm{A}, \mathrm{B}$. H_0 is the off-diagonal term, which describes the hopping of electrons from site to site through the hopping integrals $\beta_{nm}(\lambda,\mu)$ which are rapidly damped (after nearest or next nearest neighbours). It is worth noticing that, eventhough the perturbation potential due to the impurity leads to a modification of the effective atomic levels and possibly of the hopping integrals, this effect will be neglected here so that $\beta_{nm}(\lambda,\mu)$ is assumed to be ij-independent. This is valid when the extension of the orbitals of the impurity is comparable to that of the bulk atoms, i.e., for similar bandwidths of the corresponding metals in the same crystallographic structure. In this framework it is possible to calculate the local densities of states $\rho_n(E)$ at the various sites n perturbed by the introduction of the impurity, in practice essentially n_0 and its first neighbours labelled nn. This can be done from the projection of the Green function: $G(z) = (z - H)^{-1}$ without resorting to any periodicity condition (n_0 can be a defect site):

$$\rho_n(E) = \lim_{\eta \to 0^+} \left[-\frac{\mathrm{Im}}{\pi} \sum_{\lambda} \langle n, \lambda | G(E + i\eta) | n, \lambda \rangle \right] \tag{6}$$

$G(z)$ writes as a continued fraction. Its coefficients are derived either from the knowledge of the p first moments μ_p of $\rho_n(E)$:

$$\mu_p(\rho_n) = \int_{-\infty}^{+\infty} E^p \rho_n(E)\, \mathrm{d}E = \sum_{\lambda} \langle n, \lambda | H^p | n, \lambda \rangle \tag{7}$$

obtained by counting paths on the lattice [39], or directly by constructing a new basis tridiagonalising H within the so-called *recursion* method [40]. The continued fraction is then terminated by the asymptotic values of the coefficients, which are related to band (and/or gap) edges and fitted to the band structure [41]. Obviously, $\rho_n(E)$ is the most precise as the number of exact coefficients is large. In this framework, the segregation energy (Eq. (4)) can be written as:

$$\Delta E^{\mathrm{seg}}_{\mathrm{chem}} = \sum_{n=n_0,nn} \left\{ \int_{-\infty}^{E_F} E \delta\rho_n(E)\, \mathrm{d}E \right\} - \delta E_{\mathrm{Coul}}, \tag{8}$$

where $\delta\rho_n(E)$ is the variation of the local densities of states in the vicinity of the impurity between the systems in which this impurity is at the surface and in the bulk. δE_{Coul} is the variation of the Coulomb energy between these two systems which has been counted twice in the integral and is given by [42]

$$\delta E_{\mathrm{Coul}} = \sum_{n=n_0,nn} \left\{ N_e \delta\varepsilon_n + \frac{1}{2} \delta N_e \delta\varepsilon_n \right\}, \tag{9}$$

where N_e is the d-band filling for the atom at site n, $\delta\varepsilon_n$ the variation of the corresponding effective atomic energy and δN_e the variation of charge. The self-consistent determination of the potential around an impurity in a metallic matrix is a very old problem which has been solved by assuming that the perturbing potential is localized on the impurity site [43]. It is then determined according to the Friedel sum rule, which ensures the global neutrality of the system. In this framework, it has been shown that the trends obeyed by the segregation energies follow qualitatively the difference in surface energies of the two components [33]. This is particularly confirmed when the solvent and the solute are not too far apart in the periodic table, i.e., when size and alloying effects are not too important. This somewhat justifies the previously described phenomenological model. Let us mention however some noticeable exceptions in some systems of the 3-d series in which correlation effects are important [33].

Finally, it is worth noticing that these impurity segregation energies can be directly measured from core level spectroscopy experiments [44]. Indeed, it can be shown by using a thermodynamical model in the framework of the equivalent core approximation that the surface core level shift undergone by atoms of atomic number Z is nothing but the segregation energy of a $(Z + 1)$ impurity in a Z-matrix [45]. As a result, the segregation energies obey the same trends along a transition series as the surface core level shifts [46]. In particular they change sign for almost half-filled d-bands [44,47].

2.1.3. Elasticity theory

The previous models essentially account for the difference in chemical bonds between the impurity and the matrix, but not for their size-mismatch. This means that the above calculations have been performed for an impurity constrained at the atomic volume of the matrix, without relaxation of the strain energy induced by this size-mismatch. An alternative way is to only consider the segregation energy of an impurity as due to the complete release of this strain energy when the impurity is moved from the bulk to the surface. In the framework of elasticity theory, it writes [48–50]:

$$\Delta E^{\mathrm{seg}}_{\mathrm{elast}} = -\frac{24\pi K G r_{\mathrm{A}} r_{\mathrm{B}} (r_{\mathrm{A}} - r_{\mathrm{B}})^2}{3K r_{\mathrm{A}} + 4G r_{\mathrm{B}}} \tag{10}$$

in which K is the bulk modulus of the impurity (with atomic radius r_{A}) and G the shear modulus of the matrix (with atomic radius r_{B}). Let us emphasize that this effect leads to segregation of the impurity in both dilute limits B(A) and A(B) in a rather symmetric way, in contradistinction with the previous chemical ones. This means that segregation due to the size effect acts similarly, whatever the sign of the size-mismatch, this result coming from the harmonic character of elasticity theory.

2.2. Concentrated alloys with interatomic potentials

The problem is obviously more complicated if one aims at studying surface segregation in concentrated alloys A_cB_{1-c} at finite temperature. Actually, in that case one has to resort to thermodynamical models (from Bragg–Williams approximation to Monte Carlo simulations) to determine the concentration profile. Then, two types of energetic models have to be developed, depending on the importance to relax the atomic structure of the system or not. In the former case, i.e., when it is necessary to take into account the coupling between atomic relaxations and surface segregation, one has to use interatomic potentials depending on the distance. They can either be empirically pairwise or present a many-body character due to their derivation from electronic structure (EAM [51], SMA [52,53], EMT [54,55]). The second type of energetic model, suited for studies on a rigid lattice, involves an Ising-like description of the energy, which can be also either completely empirical or justified from the electronic structure. Indeed a recent derivation of an effective Ising model from the electronic structure (TBIM: tight binding Ising model [56]), in order to study surface segregation, has allowed an unified approach. In particular it validates the empirical three effects' rule [4], which states that surface segregation is controlled by the difference in surface energies between pure metals, the alloying effect and the size-mismatch one.

2.2.1. Tight-binding second moment approximation (SMA)

The tight-binding hamiltonian for an alloy A_cB_{1-c} can be written for a given chemical configuration $\{p^i_n\}$ as a generalisation of the one for a single impurity Eq. (5):

$$H(\{p^i_n\}) = \sum_i \left[\sum_{n,\lambda} |n,\lambda\rangle p^i_n (\varepsilon^i(\lambda) + \alpha^i(\lambda)) \langle n,\lambda| \right] + \sum_{i,j} \left[\sum_{n,m,\lambda,\mu} |n,\lambda\rangle p^i_n \beta^{ij}_{nm}(\lambda,\mu) p^j_m \langle m,\mu| \right]. \tag{11}$$

Let us note that this hamiltonian now accounts for "chemical disorder" by the way of two terms: a "diagonal disorder" coming from the variation of the atomic level ε^i as a function of the element and an "off-diagonal disorder" due to the difference in bandwidth or atomic radius between the two constituents, which implies an ij-dependence of the hopping integrals β^{ij}_{nm}. The local density of states at a site n occupied by an atom of the i-type $\rho^i_n(E)$ can also be obtained from the extension of Eq. (6) and the total energy of the system can be decomposed into local contributions on each site:

$$E_{\mathrm{tot}}(\{p^l_k\}) = \sum_n \left\{ \sum_{i=A,B} p^i_n E^i_n(\{p^l_k\}) \right\}, \tag{12}$$

where the local energy E^i_n results from the sum of two contributions: an attractive one obtained by integrating the density of states $\rho^i_n(E)$, and a repulsive one of the Born–Mayer type accounting for the repulsion between ions [39]:

$$E^i_n = \int_{-\infty}^{E_F} E \rho^i_n(E, \{p^l_k\})\, \mathrm{d}E + \sum_{m,j} p^j_m A_{ij} \mathrm{e}^{-p_{ij}((r_{nm}/r^{ij}_0)-1)}. \tag{13}$$

Due to the complex dependence of the density of states with $\{p_k^l\}$, the band term cannot be written as a sum of pair interactions. However, the actual density can be approximated by a schematic one with the same second moment as the real one. In this scheme the band term appears as the square root of such a sum of pair interactions [39,53,57]:

$$E_n^i = -\sqrt{\sum_{\substack{m,j \\ r_{nm}<r_c}} p_m^j \beta_{ij}^2 e^{-2q_{ij}((r_{nm}/r_0^{ij})-1)}} + \sum_{\substack{m,j \\ r_{nm}<r_c}} p_m^j A_{ij} e^{-p_{ij}((r_{nm}/r_0^{ij})-1)}, \tag{14}$$

where r_{nm} is the distance between sites n and m, r_c is the cut-off of the interaction (often taken beyond second neighbours) and r_0^{ii} the first neighbour distance in metal i ($r_0^{ij} = (r_0^{ii} + r_0^{jj})/2$). Therefore, the energy depends on three sets of parameters $\{\beta_{ij},\ A_{ij},\ p_{ij},\ q_{ij}\}$ which characterize the A–A, B–B and A–B interactions. The values of these parameters are determined for homoatomic interactions (A–A and B–B) by fitting the experimental values of the cohesive energy, lattice parameter and the so-called universal equation [58–61]. The mixed interactions (A–B) are determined to reproduce the essential feature of the A–B phase diagram, namely the existence of either a miscibility gap or ordered compounds, which is achieved by fitting the solution energies of both A in B and B in A after relaxation [62].

It is worth noticing that this SMA-potential is very similar to those derived within the embedded atom model [63,64] or within the glue model [65,66]. Its main advantage compared to the latter is its physical transparency which clearly shows its limitations... and then its possible improvements by increasing the number of exact moments. In particular some physical properties are clearly out of the scope of such simplified model. This is the case of shear elastic constants, which depend significantly on the number of moments used. In the SMA, it is found too weak for bcc metals with $Ne = 4$ (V, Nb and Ta) and too large for fcc ones around $Ne = 8$ [67].

Due to the broken bonds, the surface atoms can undergo displacements with respect to their bulk positions. In all cases, there is at least a vertical relaxation, which is experimentally known to be *inwards*, corresponding to a contraction of the first interlayer distance, for transition metals [68]. This is a first success of SMA-potentials to reproduce this contraction contrary to simple pair potential models which predict an *outwards* relaxation [69,70]. This comes from the stronger decrease with coordination Z^{tot} of the repulsive term compared to the attractive one ($\sim \sqrt{Z^{tot}}$). One has then to use such many body potentials if one aims at studying surface atomic rearrangements. Moreover, in some cases, not only vertical but also lateral atomic rearrangements can occur, changing the two-dimensional periodicity and leading to so-called surface reconstructions [71,72]. Such phenomena have to be properly predicted within the used interatomic potentials [72–74] in order to account for the possible coupling between surface segregation and reconstruction, as will be detailed in the last section.

2.2.2. Tight-binding Ising model (TBIM)

Eventhough modelling atomic relaxation of a bimetallic surface for a given chemical configuration with the previous potential is justified, using it to determine the chemical configuration, in particular the concentration profile, at thermodynamic equilibrium can be criticized. Indeed, when not only structural but also chemical rearrangements occur, the latter are essentially governed by diagonal disorder, which requires to go beyond the second moment approximation [75]. Indeed, to be sensitive to chemical configuration in terms of moments, it is necessary to check the nature of both the atoms of a given pair $n - m$, which requires two on-site hoppings involving $\varepsilon^i, \varepsilon^j$, and to go and come back from one site to the other involving twice the hopping integral: $\beta_{nm}\beta_{mn}$. The minimum approximation is then the fourth moment one and it has been shown that the fifth moment is often necessary to reproduce quantitatively the energy difference between various ordered structures in transition metal alloys [75,76]. It is then useful to develop an other type of approximation, which will only be suited to study the effect of chemical ordering on a rigid lattice. As for pure metals, the total energy of the alloy for a given

configuration cannot be described as a sum of pair interactions. Nevertheless, the small part of the energy which depends explicitly on configuration and is then the essential one in ordering problems, can be written in an Ising-like form. This is obtained by developing the energy in a perturbative way [77] with respect to that of the disordered state ($\bar{E}(c)$), described within the coherent potential approximation (CPA) [78]. In presence of a surface, preserving correctly the charge self-consistency (which reduces in most cases to a local charge neutrality rule [33]), one obtains the so-called tight-binding Ising model (TBIM) [56,79]:

$$E_{\mathrm{coh}}(\{p_n^i\}) = \bar{E}(c) + H^{\mathrm{mix}}(\{p_n^i\}), \tag{15}$$

$$H^{\mathrm{mix}}(\{p_n^i\}) = \sum_{n,i} p_n^i h_n^i + \frac{1}{2}\sum_{n,m,i,j} p_n^i p_m^j V_{nm}^{ij},$$

in which a linear term and a quadratic one appear [56]:

$$h_n^i = \frac{\mathrm{Im}}{\pi}\int^{E_F} \mathrm{d}E \sum_{\lambda} \log[1-(\varepsilon^i - \sigma_n(E))\bar{G}_{nn}^{\lambda\lambda}(E)], \tag{16}$$

$$V_{nm}^{ij} = -\frac{\mathrm{Im}}{\pi}\int^{E_F} \mathrm{d}E t_n^i(E) t_m^j(E) \sum_{\lambda\mu} \bar{G}_{nm}^{\lambda\mu}(E)\bar{G}_{mn}^{\mu\lambda}(E), \tag{17}$$

in which $\bar{G}_{nm}^{\lambda\mu}(E) = \langle n\lambda|\bar{G}(E)|m\mu\rangle$ are interatomic average Green functions, calculated from the electronic structure of the disordered state in the CPA approximation. $\sigma(z)$ is the effective potential (replacing ε^i) determined from the self-consistency CPA condition [78]:

$$\sum_i c^i t_n^i(E) = 0 \quad \text{with} \quad t_n^i(E) = \frac{\varepsilon^i - \sigma(E)}{1-(\varepsilon^i-\sigma(E))\sum_{\lambda}\bar{G}_{nn}^{\lambda\lambda}(E)}. \tag{18}$$

In all the surface segregation problems, the elementary energy balance is the previously defined segregation energy, which accounts for the exchange of a A bulk atom with a B surface one. For a given concentration profile $\{c_p\}$, where c_p is the concentration in the pth plane parallel to the surface ($p=0$), this energy writes:

$$\Delta E_p^{\mathrm{TBIM}} = \Delta h_p + \sum_i \left\{ (1-2c) Z_i^{\mathrm{tot}} V_i - \sum_{p'=-q-p}^{p'=+q-p} (1-2c_{p+p'}) Z_i^{p,p+p'} V_i^{p,p+p'} \right\} \tag{19a}$$

with:

$$\Delta h_p = (h_p^{\mathrm{A}} - h_p^{\mathrm{B}}) - (h_{\mathrm{bulk}}^{\mathrm{A}} - h_{\mathrm{bulk}}^{\mathrm{B}}) \quad \text{and} \quad V_{nm} = \frac{(V_{nm}^{\mathrm{AA}} + V_{nm}^{\mathrm{BB}} - 2V_{nm}^{\mathrm{AB}})}{2}, \tag{19b}$$

in which each atom of the p-plane has Z_i^p ($= Z_i^{\mathrm{tot}}$ in the bulk) ith-neighbours among which $Z_i^{p,q}$ in the q-plane. $V_i^{p,q}$ is the value of the "effective" alloy pair interaction V_{nm} for sites n and m ith-neighbours belonging to planes p and q, respectively.

V_{nm} decreases rapidly with the distance $(n-m)$: thus, in the fcc structure, $V_1 \gg V_2,\ V_3,\ V_4 \gg V_5, \ldots$ [80], in which case the V_1 sign indicates the tendency to order ($V_1 > 0$) or to phase separate ($V_1 < 0$) [76]. At the surface, these effective pair interactions are enhanced with respect to the bulk ones by a factor 1.5–2 [56]. This is directly related to the corresponding narrowing of the d-band [79].

The local term Δh_p, is only significant at the surface plane ($p=0$) and vanishes in the bulk ($p \gg 0$). At the surface it is almost identical to the difference in surface energies ($\tau^{\mathrm{A}} - \tau^{\mathrm{B}}$) [56], which can be interpreted with simple moment arguments [79]. In fact, Δh_0 is the main driving force which leads to the segregation of

the element with the lowest surface energy, justifying the success of the phenomenological approach previously described.

2.2.3. Size-mismatch: link between SMA and TBIM

Let us note that, up to now, the derivation of TBIM has been performed on a rigid lattice, which is probably too crude in the case of large size-mismatch between the constituents. However, it is possible to introduce this effect by adding a third contribution to the segregation energy:

$$\Delta E_p = \Delta E_p^{\mathrm{TBIM}} + \Delta E_p^{\mathrm{size}}(c). \tag{20}$$

This size-mismatch contribution is restricted to the first surface planes: $\Delta E_p^{\mathrm{size}}(c) \neq 0$ if $p = 0$ or 1 for open surfaces. $\Delta E_0^{\mathrm{size}}(c)$ is calculated in both dilute limits ($c \to 0, 1$) in the framework of SMA, by determining the four mixed A–B parameters in order that A and B only differ by their size [81,82]. This is numerically achieved by taking the matrix parameters for all interactions (AA, BB and AB), except for r_0^{ii} and r_0^{jj} which are fitted to the experimental values. This gives a contribution which significantly differs from the one derived from elasticity theory. Actually the latter leads in both limits to the segregation of the impurity, whatever its size. On the contrary, the tight-binding evaluation is found strongly asymmetric, at least for close-packed surfaces such as fcc (1 1 1) or (1 0 0). It induces a segregation of the impurity when it is the largest only [82]. This comes from the anharmonicity of the potential which exhibits a strong asymmetry between tensile and compressive strain [83,84]. However, let us note that the calculations performed for more open surfaces, such as fcc (1 1 0), leads to more symmetrical results. In this case, due to the large relaxation of the first interlayer spacing, segregation of the impurity occurs in both dilute limits as in elasticity treatment.

In all cases, the calculation being performed in both dilute limits only, one has to interpolate it for finite concentration (see Fig. 1), which is achieved as follows:

$$\Delta E_p^{\mathrm{size}}(c) = \frac{[\Delta E_p^{\mathrm{size}}(1) - \Delta E_p^{\mathrm{size}}(0)]\sin[\pi(c-0.5)] + [\Delta E_p^{\mathrm{size}}(1) + \Delta E_p^{\mathrm{size}}(0)]}{2}. \tag{21}$$

In fact the additivity in Eq. (20) is far from being justified. Moreover, this is only a partial way to introduce relaxation effects, because reconstructions and superstructure formation are not taken

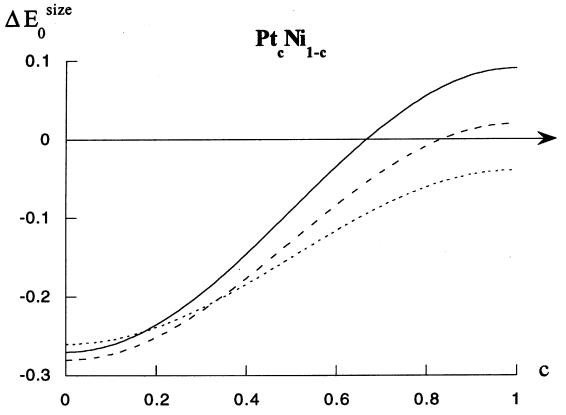

Fig. 1. Size effect contribution $\Delta E_0^{\mathrm{size}}(c)$ calculated from Eq. (21) in the particular case of the Pt_cNi_{1-c} system as a function of the surface orientation: dotted line for (1 1 1), dashed line for (1 0 0) and full line for (1 1 0).

into account. Thus, one has the choice between favouring the proper treatment of either atomic relaxation at the expense of electronic structure (using SMA-like methods though alloying effects on a rigid lattice requires to go beyond the 4th moment), or electronic structure and alloying effects against relaxations.

2.2.4. Link between SMA-TBIM and LMTO

In spite of this pessimistic alternative, one can hope to relate as consistently as possible the two methods, TBIM and SMA, both concerning the additivity of size effect, and the main properties of the V interactions. Moreover, once linked these two semi-empirical methods, it would make us confident to compare them, if possible, to ab initio calculations such the LMTO method.

Let us first comment on the connection between SMA and TBIM, i.e., on the separation between atomic and chemical structure rearrangements. Concerning the rather ad hoc treatment of the size effect term in TBIM, comparison with calculations of the segregation energy, using complete SMA calculations in the dilute limit, confirms that the approximation used is quite justified [85,86]. The situation is less clear with respect to the overall consistency between TBIM and SMA, particularly in what concerns the effective off-diagonal disorder introduced in the latter to describe alloying problems. In particular, fitting the mixed parameters on solution energies in both dilute limits does not insure that more local ordering properties are preserved. This is illustrated by calculating V (in the TBIM spirit) either from the energy of dissolution of a single impurity, or by moving two isolated impurities towards first neighbour positions. This has been simulated within SMA, for two systems presenting a significant size-mismatch and a tendency to order (CuPd) on one hand and to phase separate (CuAg) on the other hand. For $V > 0$ (CuPd), one indeed recovers the same effective V interaction as from solution energy. Moreover, performing the calculation for surface sites leads to the TBIM predicted enhancement of the pair interaction $V_0 \sim 1.5\ V$ [85]. On the contrary, for $V < 0$, one finds a sign reversal between both calculations (one or two impurities) when relaxations are not taken into account. The right sign is recovered when the atomic positions around the sites occupied by the impurities are allowed to relax [86,87]. This illustrates the intimate correlation between chemical and structural effects, at least in presence of a strong size-mismatch. Note that all these results, concerning both the justification of the TBIM partition and the essential influence of relaxation on effective pair interactions, are corroborated by FP-LMTO calculations. Finally, the effect of the surface on the effective pair interactions in the latter case ($V < 0$, large size-mismatch) is more complex than the simple TBIM enhancement ($V_0 > V$), since V_0 can even change sign with respect to V [86,87]. Indeed, the system is found to reverse its phase separation tendency towards ordering at the surface provided that a sufficient large number of bonds is broken [87].

Once granted the ability of TB-potentials, it is worth pointing out that one has to take some caution before using them. First of all, let us recall that derivation of the above TB-potentials requires drastic assumptions concerning charge neutrality near the defects (surface, impurities) [60]. For pure metal surfaces, it is now admitted that, at least for d electrons, the charge self-consistency indeed reduces to a local neutrality condition which determines a modification of the level $\delta\epsilon_0$ [42]. This d level shift is almost rigidly followed by the core levels, as experimentally confirmed by core level spectroscopy [44]. However, for fcc elements at the end of the transition series, it is necessary to introduce sp-d hybridization. This is possible in the tight-binding framework, but the energy calculations strongly depend on the charge neutrality assumption [85]. Ab initio (FP-LMTO) calculations in the surface selvedge indicate that charge neutrality has to be achieved, not only per inequivalent site but also per orbital, which means that almost no charge redistribution occurs between sp and d orbitals [88]. For alloy surfaces it is still more complicated since charge transfers are involved not only between cristallographic inequivalent sites but also between A and B species. From this point of view let us note that the use of the grand-canonical ensemble is an efficient way to cancel all charge terms to lowest order in the grand potential [76,89], as it is performed in the derivation of the TBIM [56].

2.2.5. As a conclusion: The three effects' rule

From the above arguments, one is able to identify the three main driving forces for surface segregation as being respectively: the difference in surface energies ($\Delta\tau$) and in size (Δr) between the two elements, and their tendency to order or to phase separate in the bulk (V). From the corresponding numerical values, it appears that the first term ($\Delta\tau$) is generally the main driving force, giving the nature of the segregating species in 95% of bimetallic systems. More precisely, among the 5% systems for which this argument is either incorrect or insufficient, one finds a single system (Zr–Fe) for which this is the size effect which prevails on the surface energy one, due to the very large size-mismatch between the two components. The other exceptions are the Pt-M systems (M = Ni, Co and Fe), for which $\Delta\tau$ is negligible so that the other two terms are now predominant. We will see in the following, that they indeed explain the complex behaviour in these systems.

3. Statistical models

Once granted the energetic model, the determination of the equilibrium concentration profile requires a minimization of the free energy. This can be performed using approximated methods, such as the mean-field ones, or "exact" numerical simulations such as the Monte Carlo technique.

3.1. Mean-field (one-site) approximation

The simplest mean-field treatment is the one-site Bragg–Williams approximation, which neglects any short-range order [76]. Moreover, the concentration profile $\{c_p\}$, where $c_p = \langle p_n \rangle$ for any site n in the pth plane parallel to the surface: $p = 0$, is assumed to be homogeneous. It is determined as the one which minimizes the free energy. If one defines the chemical potential as $\mu = \mu^{\mathrm{A}} - \mu^{\mathrm{B}}$ and denotes N_p the number of atoms in the p-plane, one can then write [79]:

$$F = \langle H^{\mathrm{mix}} \rangle - TS - \sum_p N_p (c_p - c)\mu, \tag{22}$$

$$\forall c_p, \quad \frac{\partial F}{\partial c_p} = 0 \;\Rightarrow\; \frac{c_p}{1 - c_p} = \frac{c}{1 - c} \exp\left(- \frac{\Delta E_p - T\Delta S_p^{\mathrm{vib}}}{kT} \right), \tag{23}$$

where the segregation energy ΔE_p is the same as defined in the previous section. It includes both the TBIM and size-effect contributions, i.e., the energy balance which accounts for the exchange of a A bulk atom with a B surface one. $\Delta S_p^{\mathrm{vib}}$ accounts for the vibrational entropy balance during the same exchange. It is generally negligible and will be omitted in the following [90,91].

It is worth noticing that the above equations are strictly valid in the disordered state, i.e., in the case where all bulk sites present the same concentration: $c_p = \langle p_n \rangle = c$. However, it is possible to account for long range order within this formalism provided that the pertinent sublattices are introduced. Thus, all ordered phases occurring on the fcc lattice can be described in terms of a few sublattices $(\alpha, \beta, \ldots)$, as illustrated in Fig. 2 for the $L1_1$ phase. In that case, the above equations can be written in terms of the concentrations per layer and per sublattice ($c_p^{\omega},\ \omega = \alpha, \beta, \ldots$), with obvious extensions of the previously defined notations:

$$\frac{c_p^{\omega}}{1 - c_p^{\omega}} = \frac{c^{\omega}}{1 - c^{\omega}} \exp\left(- \frac{\Delta E_p^{\omega}\left(c_{p-1}^{\omega'=\alpha,\beta,\gamma,\delta}, c_p^{\omega'=\alpha,\beta,\gamma,\delta}, c_{p+1}^{\omega'=\alpha,\beta,\gamma,\delta} \right)}{kT} \right), \tag{24}$$

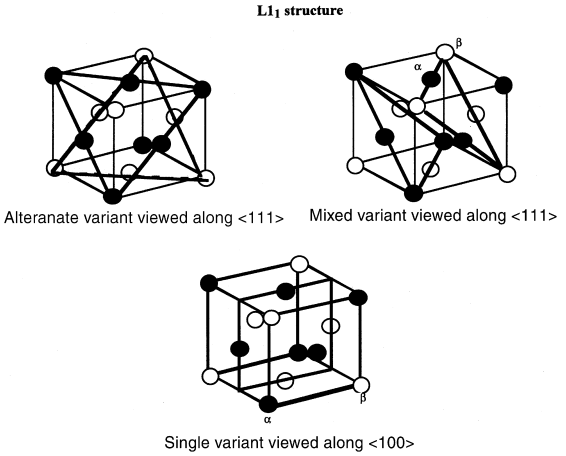

Fig. 2. Schematics of the different variants involved in the $L1_1$ fcc ordered structure, depending on the direction along which they are analyzed. α and β are the corresponding sublattices accounting for long range order effects in the mean-field Eq. (24).

$$\Delta E_p^{\omega} = \Delta h_p + \Delta E_p^{\text{size}} + \sum_{\omega'} (1 - c^{\omega'}) Z_{\text{tot}}^{\omega,\omega'} V - \sum_{p'=-q-p}^{p'=+q-p} \left\{ \sum_{\omega'} (1 - 2c_{p+p'}^{\omega'}) Z_{p,p+p'}^{\omega,\omega'} V_{p,p+p'} \right\}.$$

Note that for simple ordered structures, which can be analysed as an alternate stacking of planes rich in one or the other species $\{\ldots/\ \mathrm{A(B)}/\ \mathrm{B(A)}/\ \mathrm{A(B)}/\ \mathrm{B(A)}/\ldots\}$, the parallel layers play the role of natural sublattices. This applies for instance to the $L1_0$ structure for fcc crystals at $c = 0.5$, if it is analyzed along the (1 0 0) orientation. Indeed, in that case, only two sublattices are required to describe the alternate stacking, which leads to bulk concentrations which only differ depending on the parity of the layer:

$$c_{2p} = c_{\alpha} = \frac{1+\eta}{2}; \quad c_{2p+1} = c_{\beta} = \frac{1-\eta}{2}. \tag{25}$$

Determining the concentration profile then requires to solve a system of nonlinear equations, coupled by means of $\Delta E_p(c_{p-q}, \ldots, c_p, \ldots, c_{p+q})$. This segregation energy depends not only on the concentration of the p-layer, but also on that of the neighbouring layers through the V term. An essential problem comes from the nonlinearity which allows many solutions to exist. Therefore, it is interesting to get at once the solution of lowest energy corresponding to the thermodynamic equilibrium and the possible metastable ones which could be stabilized under variation of external parameters (pressure, temperature), leading to phase transitions. One has then to solve this system for a sufficiently large number (P) of equations giving the concentrations c_p different from the bulk one which has to be reached when $P \to \infty$. This can be achieved in the framework of techniques such as phase portrait [92,93], local field [79] or kinetic [94,95] methods.

3.1.1. Area preserving map algorithm

If we consider a coupling limited to adjacent layers, for instance for effective pair interactions limited to nearest neighbours and for sufficiently close-packed surface, one can extract c_{p+1} from the $\Delta E_p(c_{p-1}, c_p, c_{p+1})$ term and re-write the Eq. (23) as:

$$c_1 = f_1(c_0), \quad c_2 = f_2(c_0, c_1), \quad c_{p+1} = f(c_{p-1}, c_p), \quad \ldots, \quad c = f(c). \tag{26}$$

Thus, the generic equation $c_{p+1} = f(c_{p-1}, c_p)$ can be written as a two-dimensional transformation T, which admits the bulk concentration c as a fixed point at least in the disordered state:

$$(c_p, c_{p+1}) = T(c_{p-1}, c_p), \quad (c, c) = T(c, c). \tag{27}$$

Hence, a nice way to solve Eq. (23) is to determine the concentration profile as satisfying both surface equations $c_1 = f_1(c_0)$ and $c_2 = f_2(c_0, c_1)$ on one hand, and converging towards the bulk fixed point through the T transformation on the other hand, so that the iterations should satisfy definite initial and final boundary conditions. In practice, the problem is that, eventhough this fixed point is the physically stable solution of the problem, at least in the disordered state, it is mathematically unstable. One has then to identify in the (c_p, c_{p+1}) map the inflowing orbits, which converge to this point [92,93]. The concentration profile will then be given as the intersection between these orbits and curves corresponding to the boundary conditions defined by surface equations. Determining the inflowing orbits is performed by linearizing the T transformation close to its fixed point ($c_p = c + \delta c_p$) which leads to the following matrix transformation:

$$\begin{pmatrix} \delta c_{p+1} \\ \delta c_p \end{pmatrix} = \begin{pmatrix} -\frac{1}{2Z'V}\left(\frac{kT}{c(1-c)} + 2ZV\right) & -1 \\ 1 & 0 \end{pmatrix} \begin{pmatrix} \delta c_p \\ \delta c_{p-1} \end{pmatrix}, \tag{28}$$

the eigenvalues of which (λ_1, λ_2) satisfy the relation $\lambda_1 \lambda_2 = 1$. Then the situation drastically differs depending on the chemical tendency of the system, i.e., on the V sign.

(a) $V > 0$: *Tendency to ordering*: Let us first analyze the situation at high temperature ($T > T_c$), i.e., in the disordered state. In that case, both eigenvalues are real, negative and such that: $|\lambda_1| < 1$ and $|\lambda_2| > 1$. The fixed point is then hyperbolic with reflection [92], and the eigenvectors associated to λ_1 and λ_2 are respectively the slopes of the inflowing and outflowing orbits towards the fixed point. Indeed the inflowing orbit is the curve obtained by iterations from a segment close to the fixed point (c, c), directed along the eigenvector associated to λ_1, and which allows to come closer and closer from this fixed point without ever reaching it. The outflowing one is obtained in the same way from any segment directed along the other eigenvector, associated to λ_2, so that one goes farther and farther from the fixed point. In practice, the inflowing orbit is obtained by iterating the reverse transformation T^{-1} or, equivalently as the symmetric from the outflowing one by the transformation $(c_p, c_{p+1}) \rightarrow (c_{p+1}, c_p)$, i.e., by symmetry with respect to the first bisector [92,93].

By drawing on the same picture the curve corresponding to the surface boundary condition $c_2 = f_2(c_0, c_1)$, one can determine the concentration profile from the first underlayer up to the bulk since the intersection obeys both bulk and surface equations. The surface concentration is then given by the relation $c_0 = f_1^{-1}(c_1)$, and the tail of the profile by the iteration along the inflowing orbit. Let us note that, due to the reflexive character of the hyperbolic fixed point, two successive iterations on the inflowing orbit lead from one side of the fixed point to the other one: there is an oscillation of the convergence towards the fixed point, as illustrated in Fig. 3. Consequently, the concentration profile is oscillatory damped up to the bulk value, in agreement with qualitative arguments for systems with tendency to order [5].

This behaviour holds down to the critical temperature T_c, below which the disordered state becomes unstable relatively to an alternate order per plane parallel to the surface. At T_c the eigenvalues become complex, so that the related orbits are elliptic around (c, c) which is now thermodynamically unstable [92,96]:

$$T_c = -\frac{2c(1-c)(Z-2Z')V}{k}. \tag{29}$$

In fact, the only ordered case which can be treated in a simple way by this technique corresponds to the $L1_0$-type alternate ordering structure previously defined in Eq. (25), in terms of the long range order parameter defined as $\eta = c_\alpha - c_\beta$. In that case (c, c) remains a fixed point, but is unstable with respect to the

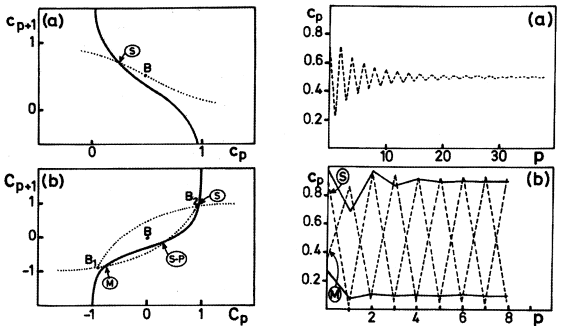

Fig. 3. Resolution of the mean-field Eq. (23) for a system with tendency to bulk ordering ($V > 0$), illustrated in the particular case of Pt_cNi_{1-c} (1 0 0) as a function of temperature. *Left-hand side*: phase portraits, including the fixed points B, B_1, B_2, their inflowing orbits (dotted lines) and the boundary condition (full line) $c_2 = f_2(c_0, c_1)$ for $c = 0.5$ and $V_0/V = 1.5$. (a) $T/T_c = 1.02$: (c_p, c_{p+1}) mapping. (b) $T/T_c = 0.61$: (C_p, C_{p+1}) mapping. *Right-hand side*: corresponding concentration profiles, using dashed lines for $c = 0.5$ and (for the sake of comparison) full ones for $c = 0.1$ and 0.9.

pair $\{(c_\alpha, c_\beta); (c_\beta, c_\alpha)\}$. One has then to find a new representation in which the fixed pair becomes a couple of fixed points. This is achieved by changing the variable "layer concentration" by the new one "order parameter" [96]:

$$c_p \to C_p = (-1)^p(2c_p - 1). \tag{30}$$

The phase portrait in the new space (C_{p-1}, C_p) presents three fixed points (see Fig. 3): the first one $(0,0)$ is elliptic and corresponds to the unstable disordered state while the two other ones (η, η) and $(-\eta, -\eta)$ are hyperbolic and account for the two possible variants of the $L1_0$ structure (A enriched planes on odd or even layers).

(b) $V < 0$: *Tendency to phase separation*: The topology of the phase portraits in the vicinity of the miscibility gap is more complex, as can be seen in Fig. 4. Indeed, there exist four different behaviours in relation with the four regions which can be identified in the corresponding bulk phase diagram, if one decreases the temperature at a given bulk concentration [93].

First, at sufficiently high temperature, the free energy presents only one minimum, corresponding to the concentration of the disordered state. (c, c) is an hyperbolic fixed point analogous to the one described in the pervious section, but now without reflection since both eigenvalues are still real but positive. Consequently, the concentration profile is monotonously damped instead of oscillatory [5].

Then, below a given temperature T_s^*, two new local extrema come in addition to the previous one: a second local minimum at a concentration c' (less stable than the one at c, and such that $c' < 0.5$ if $c > 0.5$, and vice-versa) and a local maximum at c''. This corresponds in the phase portrait to the appearance of a new hyperbolic point (c', c'), which develops a so-called homoclinic orbit around the third elliptic (complex eigenvalues) fixed point (c'', c'') [92,93]. Let us mention that $c' \neq 1 - c$ and $c'' \neq 0.5$. The temperature T_s^* is determined from the condition $c' = c''$. This region where the absolute minimum c coexists with a local one c' extends from T_s^* down to the critical temperature of phase separation T_c. This latter temperature is then given by the equality of the free energies corresponding to c and c', (which satisfy: $c' = 1 - c$ and $c'' = 0.5$), which leads to:

$$kT_c = \frac{1 - 2c}{\log\left(\frac{c}{1-c}\right)}(Z + 2Z')V. \tag{31}$$

The third region where the alloy is phase separated extends from T_c down to the spinodal temperature T_s. In this region, the free energy is characterized by the coexistence of two symmetrical minima c_1 and

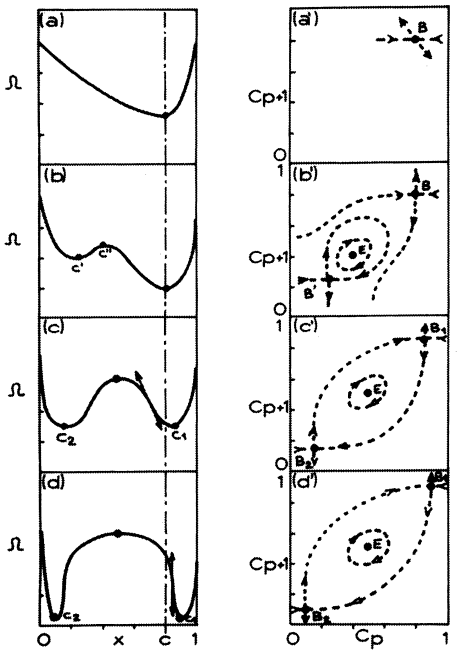

Fig. 4. Schematic evolution of the grand canonical energy $\Omega(x,T)$, for a system with tendency to bulk phase separation ($V<0$), as a function of both concentration x and temperature T: (a) $T>T_s^*$; (b) $T_s^*>T>T_c$; (c) $T_c>T>T_s$; (d) $T_s>T$. The corresponding phase portraits are given in (a′), (b′), (c′), (d′), including the fixed points with their inflowing and outflowing orbits.

$c_2=1-c_1$, the bulk concentration c being located between them in the convex part of the energy vs concentration. While the elliptic point is locked in (0.5, 0.5), the hyperbolic points (c,c) and (c',c') move to new ones (c_1,c_1) and (c_2,c_2). The inflowing orbit of one point becomes the outflowing of the other, so that the two latter fixed points are now joined by this so-called heteroclinic orbits [92,93]. Let us note that the eigenvalues associated to the (no longer) fixed point (c,c) are still real and positive. At sufficiently low temperature ($c_2\to 0$), the solubility limits can be derived from the above equation:

$$c_2=1-c_1=\exp\left[\frac{(Z+2Z')V}{kT_c}\right]. \tag{32}$$

The lower limit of this region T_s is given by the change of curvature of the free energy:

$$kT_s=-2c(1-c)(Z+2Z')V. \tag{33}$$

Here begins the domain of the spinodal decomposition where the bulk concentration c is now located in the concave part of the free energy, near the local maximum at $c''=0.5$. At first glance, no change is observed in the phase portrait. Indeed, the only modification does not come from the topological nature of the fixed points but from that of (c,c), the eigenvalues of which are now complex [93].

(c) *Advantages and limitations*: The main advantage of this technique is to visualize in an exhaustive way the whole set of concentration profiles which are solutions of the system Eq. (23). One then gets not only the most stable profile but also the metastable ones which could be stabilized, through surface phase transitions, under the modification of external parameters such as bulk concentration or temperature. One first limitation is that it does not apply to ordered systems other than those of the $L1_0$ type. An other major drawback is the bidimensional character of the phase portrait, which limits its simplicity to close-packed surfaces only, which are only linked to their adjacent layers through first neighbour interactions, at least if

one aims at avoiding to work in a multidimensional space [97]! In particular it does not work to the (1 1 0) face which then requires resorting to other techniques.

3.1.2. Local field relaxation

In the case where the p-layer interacts with more than its two adjacent planes, it is still possible to extract c_{p+q} from the rhs member of Eq. (23) in order to express it in terms of $c_{p+q-1}, c_{p+q-2}, \ldots, c_p, \ldots, c_{p-q}$ but it is not very useful. A better way is to extract c_p from the lhs of this equation, which leads to:

$$c_p = \frac{1}{1 + \frac{1-c}{c}\ \exp\frac{\Delta E_p(c_{p-q},\ldots,c_p,\ldots,c_{p+q})}{kT}}. \tag{34}$$

This system can be solved using an iterative local field technique [79]. At the kth iteration an atom in the pth layer is merged in the effective field produced by the profile $\{c_0(k),\ c_1(k),\ldots,c_{p-1}(k),\ c_p(k-1),\ldots,c_{N-1}(k-1),\ c_N(k-1), c, c, c, \ldots\}$ calculated at the previous iteration step $(k-1)$ for $c_{q>p-1}$ and at the same step for $c_{q<p}$. The new value $c_p(k)$ is then obtained by introducing this effective field into Eq. (34). From a given initial set $\{c_p(0)\}$, the process is iterated up to its convergence. Unfortunately, this technique presents the following drawback. It does not converge outside the range of temperature and concentration defined by [95]

$$c_0(1-c_0) < \frac{kT}{2Z|V|}. \tag{35}$$

Moreover, it is not exhaustive and one can miss some solutions. It is then tempting to find a technique which does not suffer all these drawbacks: it is detailed in the following.

3.1.3. Kinetic algorithm

The best way to define an iterative procedure converging towards the equilibrium state whatever concentration and temperature is to define a physical iteration process describing the evolution of the system from out-of-equilibrium towards equilibrium. This is achieved by identifying this equilibrium profile to the steady state $\{\mathrm{d}c_p/\mathrm{d}t = 0\}$ of the kinetic process which gives the temporal evolution of the concentration profile $\{c_p(t)\}$. This is performed through detailed balance equations involving the exchange fluxes between A and B atoms incoming to and outcoming from the p-layer [98]:

$$\begin{aligned}
\frac{\mathrm{d}c_0}{\mathrm{d}t} &= \frac{Z'D}{a^2}\left\{(1-c_0)c_1\ \exp\frac{\Delta E_1 - \Delta E_0}{2kT} - (1-c_1)c_0\ \exp\frac{\Delta E_0 - \Delta E_1}{2kT}\right\},\\
\frac{\mathrm{d}c_p}{\mathrm{d}t} &= \frac{Z'D}{a^2}\left\{(1-c_p)\left[c_{p-1}\ \exp\frac{\Delta E_{p-1} - \Delta E_p}{2kT} + c_{p+1}\ \exp\frac{\Delta E_{p+1} - \Delta E_p}{2kT}\right]\right.\\
&\quad \left. - c_p\left[(1-c_{p-1})\exp\frac{\Delta E_p - \Delta E_{p-1}}{2kT} + (1-c_{p+1})\exp\frac{\Delta E_p - \Delta E_{p+1}}{2kT}\right]\right\},
\end{aligned} \tag{36}$$

in which a is the lattice parameter and D the bulk diffusion coefficient, assumed to be concentration independent. In practice, a finite number (N) of equations has to be considered which has to be linked to a bulk boundary condition. In the disordered state, it is fixed to $c_{p>N} = c$. In the ordered one, it is more suited to solve the system for a slab sufficiently thick to recover bulk properties in the mid layers [98]. However, as for the real kinetic path, the obtained steady state can be a metastable equilibrium state. It is then well advised to start from different initial conditions to obtain other possible steady states.

3.2. Monte Carlo

It is possible to study the equilibrium alloy segregation beyond the mean-field approximation by taking into account all the correlation functions. This can be performed by means of Monte Carlo numerical

simulations, in conjunction with the energetics provided by either the TBIM or the SMA model. The simplest way is to consider a rigid lattice on which atoms A and B are initially randomly distributed with a given concentration. The equilibrium state is then reached by proposing either exchanges between A and B atoms of the box in the canonical ensemble, or between an atom A of the box and a B one coming from a reservoir characterized by the pertinent chemical potential in the grand canonical ensemble. Note that the latter allows us to fix the bulk concentration. Then, in the simplest Metropolis framework, the exchanges are accepted either in all cases if the corresponding energy balance ΔE is negative, or with a probability $\exp(-\Delta E/kT)$ if it is positive [99]. This insures to reach a Boltzmann configuration distribution at equilibrium.

It is worth noticing that improvements can be introduced into this simplest version of the algorithm, by including possible atomic displacements to go beyond the rigid lattice approximation [100], or constitutive vacancies to treat off-stoichiometric compounds [101]. A main advantage of the method is that it is exact from the statistical point of view. Moreover, when atomic displacements are taken into account, it allows to treat the possible coupling between crystallographic and chemical structures, therefore between reconstructions and segregation. Moreover, it accounts for anharmonicity and vibrations [102]. However, its purely numerical feature leads to long computational time and does not allow any qualitative interpretation in terms of analytic models. In addition, an exhaustive description of the whole set of possible situations is very tedious. In that context, an approach which is well-suited to surface segregation studies is to use successively the mean-field approximation within the TBIM energetic model to classify the various possible behaviours, and then Monte Carlo simulations, both in the TBIM and SMA frameworks, for getting more quantitative results.

3.3. Alternative approaches

We present only very briefly some alternative approaches in the following. An exhaustive review of each method is clearly out of the scope of the present paper. However, we give some important references for each approach and we invite the reader to refer to them.

3.3.1. CVM

Even in the framework of the mean-field approximation, it is possible to go beyond the one-site Bragg–Williams approximation by including short-range order in sufficiently large clusters (pairs, triangles, tetrahedra, ...) to account for the possible frustrations due to the lattice structure [103]. In particular the bulk phase diagram is largely improved in fcc structure with ordering tendency when using the cluster variation method (CVM) [76]. Its use for surface segregation studies is still not much developed [104–107].

3.3.2. Landau development

An analytic treatment, which is particularly useful to study the interrelation between bulk and surface phase transitions, is based on Landau expansion of the free energy. This is an elegant and efficient way to discuss the role of the temperature, the surface local field and the variation of the effective pair interactions at the surface on the surface phase transition [92,108–113].

3.3.3. Mean-field method on relaxed lattice

This method is based upon the Bragg–Williams approximation for the configurational entropy and an Einstein model for vibrational contributions to the free energy [114]. Using any type of description of atomic interactions, the free energy is minimized with respect to atomic coordinates and composition of each site. Thus atomic structure and segregation are determined in a more efficient way than in pure numerical methods such as Monte Carlo but the approximations are not well controlled [102] and the analytical character of the mean-field method on rigid lattice is not conserved. However, the results obtained by

this method and Monte Carlo simulations are generally in good agreement both for surface and grain boundary segregation [115,116].

4. Surface segregation in the solid solution

4.1. Generalities

Let us first try to show, in a schematic way, how the three previously identified driving forces act upon the segregation isotherm at high temperature, by looking in more details at the segregation energy given by Eqs. (19a) and (19b). For the sake of simplicity, let us re-write these energies for a close-packed surface with effective pair interactions limited to first neighbours and unchanged at the surface ($V_0 = V$):

$$\begin{aligned}\Delta E_0 &= \Delta h_0 + \Delta E_0^{\text{size}} + Z'V + 2V[Z(c_0 - c) + Z'(c_1 - 2c)],\\ \Delta E_1 &= 2V[Z(c_1 - c) + Z'(c_0 + c_2 - 2c)],\\ \Delta E_p &= 2V[Z(c_p - c) + Z'(c_{p-1} + c_{p+1} - 2c)].\end{aligned} \tag{37a}$$

Moreover, let us assume in a first step that the surface enrichment is driven, as it is generally the case, by the two local fields related to the difference in surface energy (Δh_0) and to the size effect (ΔE_0^{size}). The alloying term being neglected, $\Delta E_0 = \Delta h_0 + \Delta E_0^{\text{size}}$ and $\Delta E_{p>0} = 0$, so that the sign of ΔE_0, and then the tendency to segregation of A or B, results from the competition between the two terms. The former one leads to segregation of the element with the lowest surface energy. The latter one, which only plays a role for sufficiently large size-mismatch, leads to segregation of the impurity when it is the largest, except for open surfaces for which it leads to segregation of impurity whatever its size. In that case, only the surface is affected by segregation.

Let us now see what is the influence of the alloying term in the few cases where both local fields can be neglected. In that case

$$\Delta E_0 = 2V[Z(c_0 - c) + Z'(c_1 - 2c + 0.5)]. \tag{37b}$$

Moreover, the sign of ΔE_0 can be analysed at the first iteration of the local field algorithm (Section 3.1.2), i.e., with $c_0 = c_1 = c$, leading to $\Delta E_0 = VZ'(1 - 2c)$. Therefore, the sign of ΔE_0 is the same as that of V if $c < 0.5$ and reversed if $c > 0.5$. This means that for a system presenting a tendency to bulk ordering ($V > 0$), the alloying term favours segregation of the majority element, whereas for a system presenting a tendency to bulk phase separation ($V < 0$) it favours segregation of the minority element. Note that, contrary to the surface energy term which is concentration independent, the alloying term changes sign with bulk concentration (similarly to size effect, at least for open surfaces). As a consequence, the alloying and size effect terms compete for $V > 0$ whereas they are synergetic for $V < 0$. It means that surface segregation should be larger for phase separation systems than for ordering ones. The influence of all these contributions are illustrated on the schematic isotherms exhibited in Fig. 5.

Once the nature of the element segregating at the surface is known, the nature of the profile is determined by the sign of the alloying term (V). Indeed, if one writes the segregation energy on the first underlayer by keeping only the surface concentration different from the bulk one ($c_1 = c_2 = c$): $\Delta E_1 = 2VZ'(c_0 - c)$. Therefore, if $V > 0$, ΔE_1 is positive (leading to $c_1 < c$) if $c_0 > c$ and negative (leading to $c_1 > c$) in the opposite case ($c_0 < c$), so that in all cases the first underlayer is depleted with respect to the species which segregates at the surface: the profile is oscillating. On the contrary, if $V < 0$, ΔE_1 is negative (leading to $c_1 > c$) if $c_0 > c$ and positive (leading to $c_1 < c$) in the opposite case ($c_0 < c$), so that in all cases the first underlayer is enriched with the same species as the surface: the profile is monotonous. To summarize, for ordering systems ($V > 0$) the first underlayer is depleted with

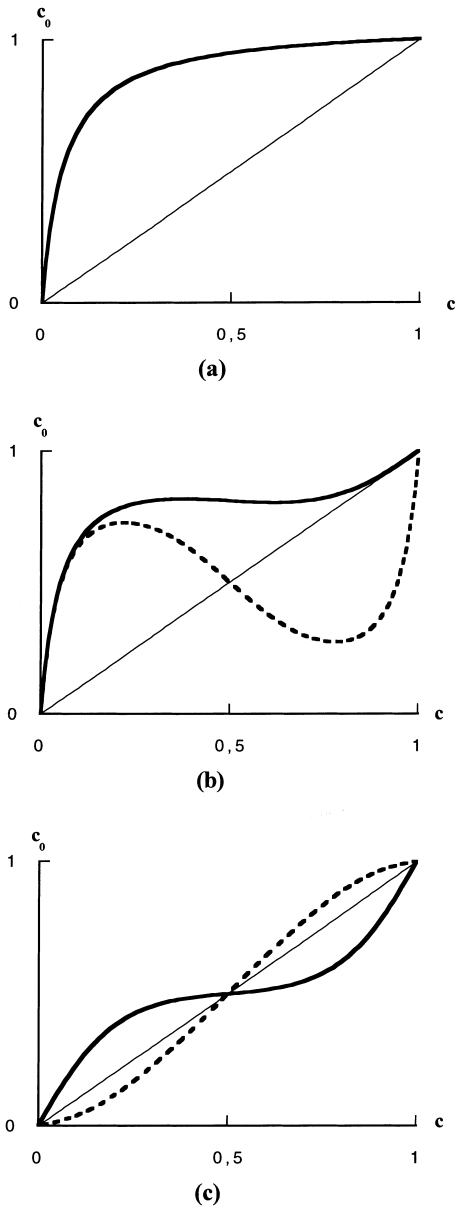

Fig. 5. Schematic isotherms illustrating the separated influence of the three TBIM driving forces for a A_cB_{1-c} system with $\Delta h_0 < 0$ (i.e., $\tau^A < \tau^B$, where τ is the surface energy) and $r^A > r^B$ (where r is the atomic radius): (a) surface energy effect ($\Delta E_0^{\text{size}}(c) = 0$, $V = 0$); (b) size effect ($\Delta h_0 = 0$, $V = 0$): the full line is obtained with $\Delta E_0^{\text{size}}(c)$ derived from Eq. (21) for close-packed surfaces (see Fig. 1) while the dotted one corresponds to elasticity-type calculations (Eq. (10)); (c) alloying effect ($\Delta h_0 = 0$, $\Delta E_0^{\text{size}}(c) = 0$): the full line is for $V < 0$ and the dotted one for $V > 0$.

respect to the segregating species (oscillating profile), whereas it is still enriched but to a lesser extent (monotonous profile) for phase separating ones. Let us recall that this result was obtained in a different way, using the phase portrait analysis (Section 3.1.1).

It remains now to determine how many layers are required to damp the profile up to bulk concentration, once the direct effects due to the surface local fields do not play a role anymore [3]. Let us assume that this damping is of the exponential type [117]:

$$c_p = c(1-\omega_p) \quad \text{with} \quad \omega_p = \Omega e^{-\lambda p}. \tag{38}$$

Introducing this expression into Eqs. (23) and (37a), and linearising the resulting equation as a function of ω_p ($\omega_p \ll 1$), one finds that the damping factor λ (complex number) obeys the equation:

$$\cosh(\lambda) = C(T) \quad \text{with} \quad C(T) = -\frac{\frac{Z}{Z'} + \frac{kT}{2VZ'c(1-c)}}{2}. \tag{39}$$

The damping behaviour of the profile drastically depends on the value of $|C(T)|$ relative to unity. More precisely, $|C(T)| > 1$ corresponds to real values of λ and therefore to a damping which indeed exponentially decreases, either monotonously ($C(T) > 1$) or in an oscillating way ($C(T) < -1$). On the contrary, $|C(T)| < 1$ leads to imaginary values of λ which reveal a nondecreasing oscillating profile. Let us analyse the implications of this result as a function of the tendency of the system to order or to phase separate.

(a) *Tendency to phase separation* ($V < 0$): In that case, the condition $C(T) > 1$ is nothing but the condition $T > T_s$, where T_s is the spinodal temperature given by Eq. (33). It means that the concentration profile is monotonous and exponentially damped in the solid solution regime. This is illustrated in Fig. 6(a) in which one verifies that the correlation length $1/\lambda$ indeed diverges at the spinodal temperature. Moreover, according to Eqs. (38) and (39), λ (and therefore the damping) is the strongest in the dilute limits ($c \to 0,\ 1$), in the high temperature regime and when the coupling between two adjacent layers is weak, either $|V|$ or Z' being small. Let us recall that the limit case $V = 0$ corresponds to the simplest case where segregation is limited to the surface layer.

(b) *Tendency to ordering* ($V > 0$): Now, the disordered state corresponds to the condition $C(T) < -1$, which means that the concentration profiles are oscillating and exponentially damped in this range, which extends down to the temperature T_c at which $1/\lambda$ diverges. T_c corresponds to the order–disorder temperature given by Eq. (29), for alternate ordered structures of the $L1_0$ type. Moreover, as can be seen in Fig. 6(b), for a same set of parameters (Z', c, $kT/|V|$), the damping is larger than for a phase separating system. Below T_c, one can still hold a similar analysis by using concentrations on the two sublattices (odd and even layers), which reveals that the damping abruptly increases leading to segregation limited to the surface layer for ordered compounds at low temperature [117].

In fact, whatever the V sign, the most interesting situation is found for intermediate temperatures, namely slightly above bulk critical temperatures. Thus, depending on the sign of V, it will be shown that either concentration profile transitions (for systems where surface local fields and alloying effect compete and $V > 0$, such as PtNi, see Section 4.2.1) or layering transitions (for systems with a strong tendency to solute segregation and $V < 0$, such as Cu(Ag), see Section 4.3) may occur. More precisely, in view of the previous results concerning the damping of the concentration profile, it appears that the relevant parameter accounting for these two types of transitions is the bulk concentration more than the tendency to order or to phase separate. Indeed, the profile transitions occur at equiconcentration when the damping is minimum whereas the layering transitions exist in the dilute limits for which the damping is the strongest.

4.2. $V > 0$: Concentration profile in the disordered state

For $V > 0$, the concentration profile can strongly depend on the respective contributions of the surface energy effect and the alloying one. In particular, if the former is not too high, it can either compete with the latter, leading to unusual anisotropy of the surface enrichment (Cu–Pt case, see Section 4.2.2), or it can be completely negligible (Pt–Ni case, see Section 4.2.1). In this last case the competition between the asymmetric size effect and the alloying one leads to "profile phase transitions" between pure Ni and pure Pt

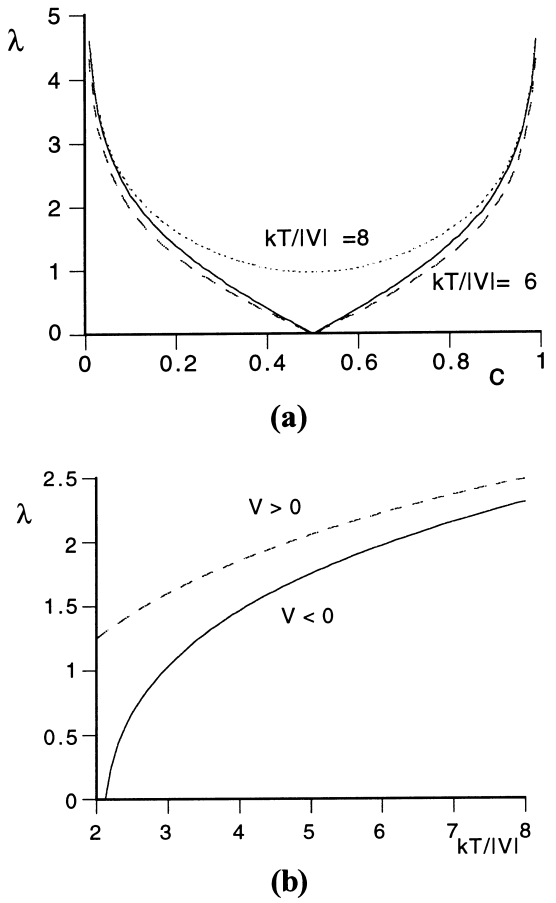

Fig. 6. (a) Damping of the concentration profile (λ) as a function of bulk concentration and temperature ($|kT/V|$) for two fcc surface orientations: (1 1 1) full line and (1 0 0) dotted and dashed lines. (b) Temperature dependence of this damping (λ) as a function of the V sign for a (1 0 0) fcc surface and a bulk concentration $c = 0.1$.

terminated surface sandwiches as a function of surface orientation, concentration and temperature [96,118–121].

4.2.1. Profile transitions in Pt_cNi_{1-c}

The energetic quantities (Δh_0, V, ΔE_0^{size}) derived from TBIM are given in Table 1 [96]. At high temperature ($T/T_c = 1.02$) the phase portrait and the concentration profile, shown in Fig. 3 for the (1 0 0) face at $c = 0.5$, exhibit only one solution which corresponds to an oscillating profile terminated by Pt at the surface. This conclusion holds in the whole range of concentration, whatever the temperature in the disordered state. This is in qualitative agreement with experiments [29], the oscillatory behaviour being somewhat underestimated by the calculations [96]. Very similar results are obtained for the (1 1 1) face, the segregation being lower, as expected for a more close-packed surface. The (1 1 0) orientation is more spectacular, as can be seen in Fig. 7 for $c = 0.5$. Indeed, at sufficiently high temperature, one still finds only one solution but which corresponds to a slight Pt-enrichment on the first two layers, then followed by the usual rapidly damped oscillations. Decreasing the temperature down to (but still above) the order–disorder temperature T_c, leads to three intersections between the boundary condition and the inflowing orbit: one

Table 1
TBIM parameters (in meV) for the bimetallic systems used as illustrations in the present paper. The two values given for the size effect refer to those calculated in both (bulk) dilute limits ($c \to 0$ and $c \to 1$). Note that, for PtSn, only the sum of the tension and size effects has been reported

		Δh_0	$\Delta E_0^{\text{size}}(0)$	$\Delta E_0^{\text{size}}(1)$	V_1	V_2
Pt_cNi_{1-c}	(1 1 1)	0	−260	−40	84	0
	(1 0 0)	0	−280	20	84	0
	(1 1 0)	0	−270	90	84	0
Cu_cPt_{1-c}	(1 1 1)	−210	60	130	20	40
	(1 0 0)	−290	20	140	20	40
Cu_cPd_{1-c}	(1 1 1)	−135	38	90	73	0
Sn_cPt_{1-c}	(1 1 1)	≈−850			192	
Ag_cCu_{1-c}	(1 1 1)	−110	−250	−20	−32	0

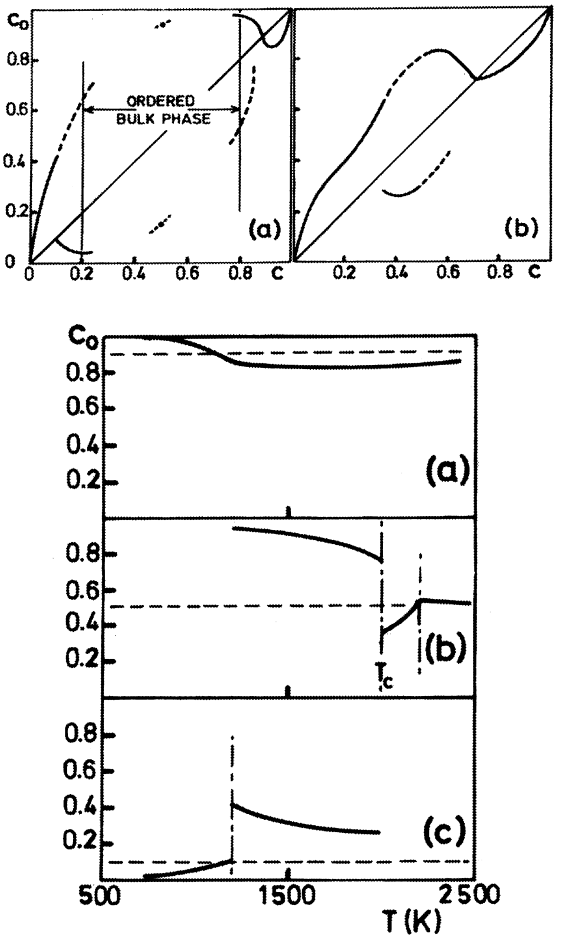

Fig. 7. Variation of the surface concentration c_0 for Pt_cNi_{1-c} (1 1 0). *Upper part*: as a function of c, for two temperatures $T/T_c^{\max} = 0.61$ (a) and 0.96 (b) ($T_c^{\max}$ is the order–disorder temperature for $c = 0.5$) and for $V_0/V = 2$. The full (dashed) line is for the stable (metastable) solution. Note that in (a), only the points corresponding to $c = 0.5$ have been calculated in the ordered region. *Lower part*: as a function of temperature for three concentrations: $c = 0.9$ (a), 0.5 (b) and 0.1 (c), in which case c_0 plays the role of a surface order parameter.

stable and one metastable solutions and a saddle point, the stable solution corresponding now to a surface Ni-enrichment in agreement with experiments. The respective stabilities of these two solutions are found to be drastically concentration dependent (Fig. 7) since, at low Pt concentration ($c = 0.1$), we predict a first order transition at $T_c^s \simeq 1140$ K between a sandwich with Ni on top for $T < T_c^s$ (as observed in LEED) and a sandwich with Pt on top for $T > T_c^s$. For $c = 0.5$, decreasing the temperature, we have first a Pt-enrichment (as mentioned above), which then switches to a *Ni*-one, after a second order transition at $T_c^s \simeq 1.1\ T_c$. Then, at the critical bulk temperature, a strongly first order surface phase transition occurs, leading to a surface enriched with Pt at lower temperature (stable termination of the ordered compound). Such a profile phase transition has indeed been experimentally observed. Finally, for high Pt concentrations (around $c = 0.9$), we obtain a crossover from a Ni-enriched surface ($T > 1150$ K) to a Pt-enriched one ($T < 1150$ K) without first order transition.

Let us emphasize that the peculiarity of the segregation in the (1 1 0) case is mainly due to the size effect. Indeed, in that case, taking into account the oscillating surface relaxation leads to a more symmetric term which favours segregation of the impurity in both dilute cases, as for elasticity. Let us recall that for more close-packed surfaces, the segregation of the impurity, only when it is the largest atom (Pt), is favoured. On the contrary, in all cases, the alloying term leads to segregation of the majority element. Therefore, since the usually leading term (difference in surface energy) is here negligible, this is the balance between the other two terms (size effect and alloying effect) which drives segregation. For close-packed surfaces, Pt segregation is driven by the size effect on the Ni-rich side and by the alloying term on the Pt-rich one. For the (1 1 0) face both effects compete on the whole range of concentration leading to the profile transitions. Note that such a behaviour should occur each time that the surface energies of the components are similar. Indeed, such a reversal of the surface sandwich is predicted for similar systems Pt–M (such as M = Ni, Co, Fe) and indeed experimentally observed [29].

4.2.2. *Peculiar anisotropy in* Cu_cPt_{1-c}

Another surprising consequence of the competition between the surface energy effect and the alloying one when the former is not too high can be a change of the usual anisotropy of surface segregation [122]. Indeed, when the leading term is, as usual, the difference in surface energies, the face dependence of surface segregation follows the anisotropy of these surface energies, i.e., the enrichment is more important for the open faces than for the close-packed ones. Thus, in fcc structure, surface segregation is expected to increase from the (1 1 1) to the (1 0 0) orientation. However, a competition can occur between the surface energy effect and the alloying term when the equiatomic alloy tends to order at low temperature in the $L1_1$ phase, i.e., along alternate stacking of pure close-packed (1 1 1) planes, the more open (1 0 0) planes being therefore mixed. In that case, one can expect, even in the disordered state, a strong variation of the anisotropy of surface segregation with temperature, favouring a larger enrichment on the (1 1 1) face relatively to the (1 0 0) one at low temperature and the inverse segregation anisotropy at higher temperature.

This is indeed what is found for the Cu_cPt_{1-c} system, which is the only transition metal alloy for which the $L1_1$ phase is observed at low temperature. Indeed, stabilizing this phase requires the second neighbour interactions to be larger than first neighbour ones ($V_2 > V_1$). Unfortunately, this is an exception to the general rule derived from TBIM calculations ($V_1 \gg V_2$ [80]), so that the only way to take this effect into account is to fit these two parameters, for instance from the mixing enthalpy and the order–disorder temperature. This leads to values given in Table 1 [95]. It is then easy to calculate the concentration profile for both orientations using the phase portrait technique for this set of parameters. The main results are illustrated by the isotherms in the disordered state ($T = 1.07\ T_c$) which are shown in Fig. 8 [122]. First, Cu segregates whatever the concentration due to the surface energy term, but there is an enhancement of the Cu enrichment when going from the open (1 0 0) face to the more close-packed (1 1 1) one (at least for $c > 0.3$), contrary to usual surface energy arguments. In addition, the concentration profile strongly differs between these two faces: it is overoscillating for (1 1 1) and abrupt for (1 0 0). All these features are

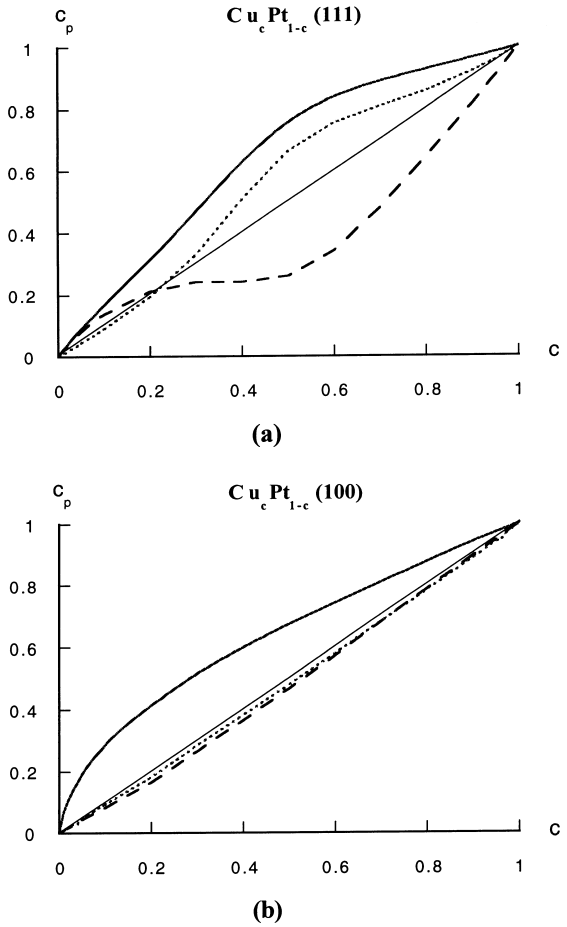

Fig. 8. Anisotropy of the segregation isotherm for Cu_cPt_{1-c} in the disordered state ($T/T_c = 1.07$) for two surface orientations. (a) (1 1 1) and (b) (1 0 0). The full, dashed and dotted lines represent respectively the concentrations c_0, c_1 and c_2.

obviously related to the competition or the synergy between the surface energy term and the alloying one. The first effect favours a surface Cu enrichment, larger for the (1 0 0) face than for the (1 1 1) one, whereas the second one leads, at low temperature in the ordered state, to pure planes along the ⟨1 1 1⟩ direction and mixed ones along ⟨1 0 0⟩. These behaviours can be more quantitatively analyzed by studying the temperature dependence of the corresponding segregation energy ΔE_0 [122]. It presents a crossover between $\Delta E_0^{(1\,1\,1)}$ and $\Delta E_0^{(1\,0\,0)}$, the usual anisotropy being recovered in the asymptotic regime of infinite temperature, whereas the unusual sequence exists in a large range of temperature, up to $T/T_c = 1.4$ for $c = 0.5$ [122]. Indeed, a detailed analysis of the expression of ΔE_0 shows that the alloying term plays against the other two terms for the (1 0 0) face whereas all the terms are synergetic for the (1 1 1) one, which confirms that the origin of the crossover is indeed the competition between the surface energy effect and the alloying one.

4.3. Layering transitions ($V < 0$): Cu(Ag)

Essentially due to the missing bonds, surface can be the place where precursor critical phenomena can occur. In particular, in pure metals, the surface premelting is one of the clearest examples [123]. We will

show here that surface can play a similar role for phase separation. Let us consider, for example, a dilute alloy with tendency to bulk phase separation. If a strong segregation of the solute enriches the surface region, a first order transition can happen at the surface, even if the bulk concentration is lower than the solubility limit at the considered temperature. This can be viewed as a pre-phase separation, located at the surface. The corresponding isotherm is referred to as being of the Fowler–Guggenheim type, for which the surface transition is due to the c_0 dependence of the segregation energy (see Eqs. (37a) and (37b)):

$$\frac{c_0}{1-c_0} = \frac{c}{1-c} \exp\left[-\frac{\Delta E_0(c_0)}{kT}\right]. \tag{40}$$

Then, when approaching the critical temperature at fixed bulk concentration, an infinite number of phase transitions can occur concerning successively each layer parallel to the surface [10]. The Ag_cCu_{1-c} alloy in the copper rich region of the phase diagram ($c \to 0$) is a candidate for this type of behaviour [124–126] because it presents a simple phase diagram with tendency to phase separation and all the energetic ingredients (ΔE_0^{size}, Δh_0 and V) lead to a strong Ag segregation, as can be seen in Table 1 [127,128]. Note that the value of V leads to a solubility limit $c_\ell^\infty = 0.012$ at $T = 1000$ K. As a consequence, in the copper rich region of the phase diagram, even when the silver bulk concentration is lower than c_ℓ^∞, the surface concentration can be largely greater than c_ℓ^∞ due to the strong silver surface segregation. This can be seen in Fig. 9, where the sum of the surface and first underlayer concentrations $c_0 + c_1$ is plotted as a function of the bulk concentration for five different temperatures, using either mean–field or Monte Carlo simulations [129]. At 2000 K the segregation isotherm does not show any first order layering transition. At 1500 and 1200 K, only one first order transition appears, in the lower part of the isotherm, the surface layer going from a Cu rich to a Ag rich concentration when the bulk concentration

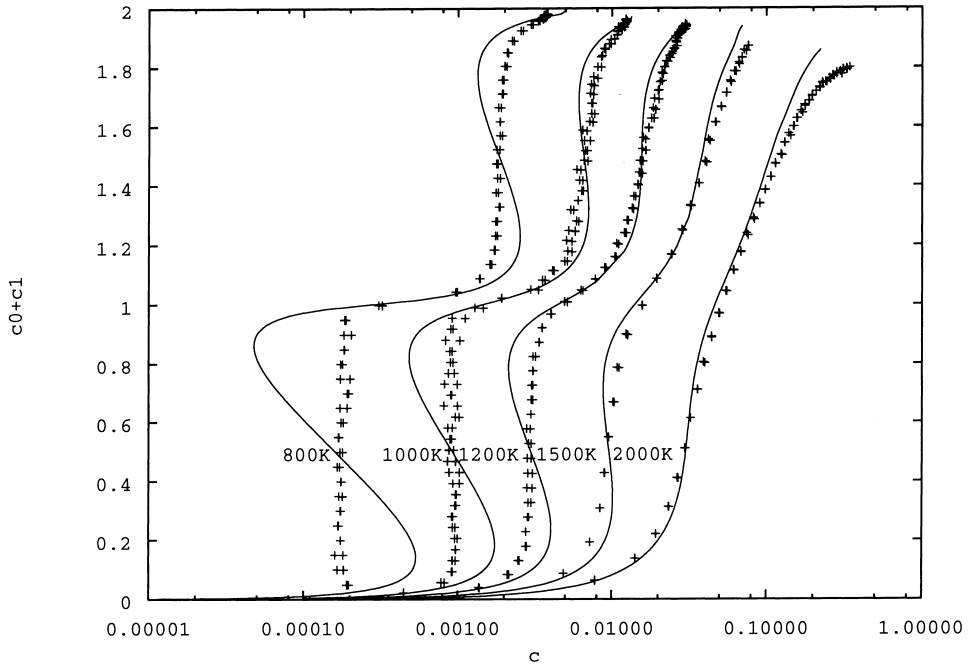

Fig. 9. Layering transitions in Ag_cCu_{1-c} (1 1 1) from mean-field (full lines) or Monte Carlo (crosses) calculations. The "extended" segregation isotherms, giving $(c_0 + c_1)$ as a function of c, are plotted at different temperatures.

reaches the limiting value $c_\ell^0 < c_\ell^\infty$. Finally, at 1000 and 800 K, there are two first order transitions. The first one, which occurs in the lower part of the isotherm and at lower bulk concentration corresponds to the transition of the surface layer. The second one, located in the higher part of the isotherm and occurring at higher bulk concentration c_1, corresponds to the transition on the first underlayer. The critical bulk concentrations c_ℓ^0 and c_ℓ^1 at which the first two layers undergo layering transition depend on temperature so that there is a limit temperature above which there is no longer first order transition for the surface plane $T_\ell^0 = -(ZV_0/2k) = 1678$ K and similarly for the first underlayer $T_\ell^1 = -(ZV/2k) = 1119$ K [127–129]. Note that, apart from the Van der Waals loops which only appear in the mean-field calculation, mean-field and Monte Carlo segregation isotherms are in good agreement. However, as usual, the Monte Carlo limiting temperatures T_ℓ^0 and T_ℓ^1 are lower: $T_\ell^0 = 1018$ and $T_\ell^1 = 679$ K than in the mean-field approximation.

For a given temperature, when c increases from $c_\ell^1(T)$ to c_ℓ^∞, the second underlayer undergoes a first order transition, then the third, etc. For each n, except the first three layers, when $c = c_\ell^n(T)$, c_n jumps from approximately 0.12 to 0.88 (at $T = 1000$ K) and concomitantly c_{n-1} and c_{n+1} make a companion transition [130]. Between two transitions when the bulk concentration lays between c_ℓ^n and c_ℓ^{n+1}, n+1 layers near the surface are rich in Ag: the first two ones with a concentration very near 1, the following ones with $c_i = 1 - c_\ell^\infty$ and finally $c_n = 0.88$. An interphase is formed because then follows a region rich in Cu with $c_{n+1} = 0.12$ and the following concentrations very near c_ℓ^∞. This concentration profile is similar to the one found in the equilibrium interphase of limiting concentrations $1 - c_\ell^\infty$ and c_ℓ^∞. Moreover, except for the layers close to the surface, the bulk concentration at which the nth layer undergoes its first order transition approaches exponentially $c_\ell^\infty(T)$ for increasing n [130]. As for the surface and subsurface layers, there is a limit temperature T_ℓ^n above which the nth layer does not undergo a first order transition. Except if the pair interaction is enhanced at the surface, in which case $T_\ell^0 > T_\ell^1$ [127,128], one finds that T_ℓ^0 is slightly lower than T_ℓ^1, this slightly lower than T_ℓ^2, etc., also $T_\ell^n \to T_c$ when $n \to \infty$ [10]. From the experimental point of view it has been shown that the mentioned transition exists at least for the surface layer [126,131,132], but the complete wetting remains to be confirmed.

5. Surface segregation in the bulk ordered state

In the previous section we have presented segregation isotherms obtained in the bulk disordered state, i.e., in the range of the bulk solid solution. The aim of the present section is to investigate the relation between these isotherms and those in the ordered state, which characterize the surface termination of a compound. Indeed, it is generally believed that the surface of a stoichiometric compound is its ideal termination, i.e., it has the same composition as an equivalent bulk plane. Such a simple idea implies a very strong effect of the crystallographic orientation of the surface. Actually, we have to distinguish the following cases [95]

- The stacking of planes parallel to the surface consists of equivalent planes of nominal composition, as for the (1 1 1) face in simple fcc ordered structures ($L1_0$ and $L1_2$): the ideal termination for the A_3B compound then corresponds to a surface composition $c_0^A = 0.75$.
- The stacking involves planes of alternate composition, as for the (1 0 0) and (1 1 0) orientations in $L1_2$ structure. For instance A_3B compound can be viewed as a stacking of $\{\ldots/A/AB/A/\ldots\}$ planes along the $\langle 1\ 0\ 0\rangle$ or $\langle 1\ 1\ 0\rangle$ directions, leading to a surface composition c_0^A equal to 1 or 0.5 depending on the ideal termination. This means that the multisolution behaviour of the segregation equilibrium could be the rule in the ordered state, at least for some surface orientations, whereas it was the exception in the disordered state.
- When the ordered structure is not built on the same lattice as the disordered one (as the quadratic $L1_0$ structure relatively to the fcc solid solution), various orientational variants can be observed, hereafter

referred to as alternate or mixed variants (see Fig. 2). For the $L1_0$ structure along $\langle 1\ 0\ 0\rangle$ direction, it corresponds respectively to the stacking $\{\ldots/A/B/A/B/\ldots\}$ and $\{\ldots/AB/AB/AB/AB/\ldots\}$ and therefore to an ideal termination of composition c_0^A equal to 1 or 0 in the first case or 0.5 in the second case.

At first sight, the relation between surface segregation in the disordered state, mainly due to the surface energy effect, and the assumed stability of the ideal termination of a compound, favoured by the alloying effect, is not clear at all. A great advantage of the mean-field approach, described in Section 3, is to allow an analytic treatment, both in the disordered and in the ordered state, leading to an understanding of the segregation driving forces in both situations. To illustrate the role of the crystallographic orientation, we will present some results obtained on the (1 1 1) and (1 0 0) faces for Cu–Pt alloys (Section 5.1). Then we will detail the behaviour of the surface segregation isotherm near bulk phase transitions for the (1 1 1) face in Cu–Pd system (Section 5.2). Finally, the role of 2-D-compounds will be illustrated in the Pt–Sn case (Section 5.3).

5.1. Role of the crystallographic orientation in Cu–Pt alloys

As already mentioned in Section 4.2.2, the Cu–Pt system is characterized by the stability of the $L1_1$ structure in a large range of concentration around 0.5, which requires to use effective pair interactions between nearest (V_1) and next-nearest neighbours (V_2). This induces an unusual anisotropy of surface segregation between the (1 1 1) and (1 0 0) faces in the disordered state [95,122]. We will show here how this extents to the $L1_1$ ordered state, by solving the mean-field Eq. (24) in the presence of the pertinent number of sublattices allowing to describe the various ordered states. More precisely, the (1 1 1) stacking in the $L1_1$ structure leads to two variants. One is alternate: $\{\ldots/Cu/Pt/Cu/Pt/\ldots\}$ with two possible ideal terminations (pure Cu or pure Pt) whereas the other is mixed: $\{\ldots/CuPt/CuPt/\ldots\}$. We show in Fig. 10 the segregation isotherms at $T = 750$ K (i.e., $T/T_c = 0.5$, where T_c is the order–disorder temperature at $c = 0.5$) for all these cases [94]:

1. The most stable composition profile corresponds to the alternate variant with the Cu-rich termination. In agreement with the results shown at higher temperature in disordered state (see Fig. 8), a Cu surface enrichment is observed in the whole range of concentration, which is strong relatively to the bulk concentration, but only slight with respect to the ideal termination (which is strictly recovered for the stoichiometric compound CuPt). The bump on the first underlayer concentration (c_1) is correlated with the occurrence of bulk ordering near $c = 0.16$. It illustrates the competition or the synergy between the surface (or subsurface) segregation driving forces and bulk ordering phenomenon.
2. The concentration profile corresponding to the alternate variant with a Pt-rich termination is only metastable (with a free energy larger by 80 meV/at for $c = 0.5$) and presents two other differences with respect to the stable Cu-rich termination. Firstly, the surface concentration strongly differs from the ideal termination one. Moreover, the existence range of this metastable solution is rather limited ($0.3 < c < 0.55$), well inside the bulk ordering range ($0.16 < c < 0.84$), becoming unstable and turning into one or the other two terminations by means of an antiphase boundary in the remaining ordered concentration range.
3. The termination of the mixed variant is slightly Cu-enriched with respect to the ideal termination, even for the equiatomic compound. Its free energy has an intermediate value lying between the ones of the two terminations of the alternate variant (larger by 10 meV/at at $c = 0.25$). This mixed variant termination becomes unstable for $c > 0.55$, being replaced by the stable Cu-rich termination followed by an antiphase boundary located on plane 8.

In order to illustrate the influence of the surface orientation in the ordered state, we present in Fig. 10 the corresponding isotherm for the (1 0 0) face. Let us recall that the stacking in the $\langle 1\ 0\ 0\rangle$ direction is rather similar to the (1 1 1) mixed variant described above, all the planes having the bulk concentration. Only one

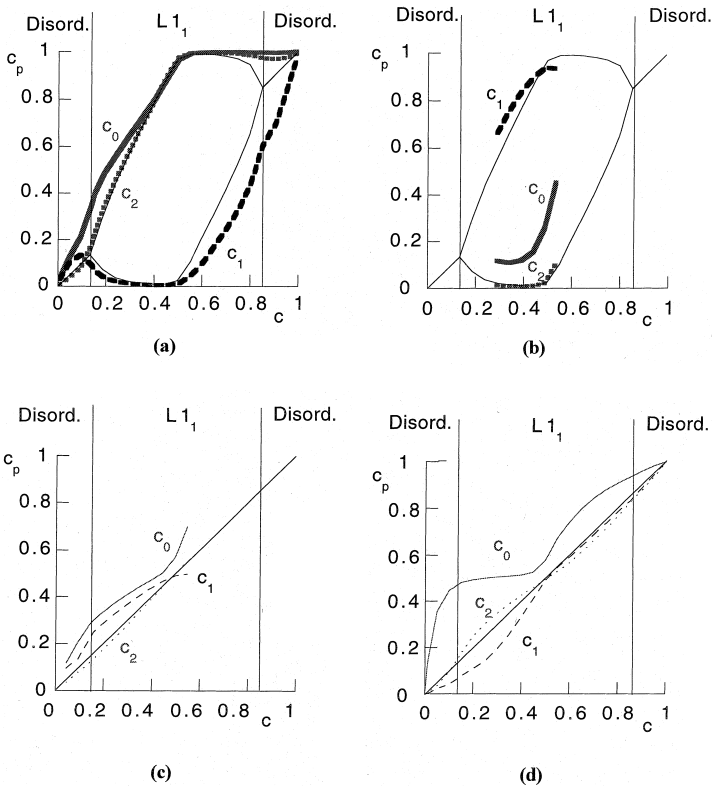

Fig. 10. Segregation isotherms for Cu_cPt_{1-c} in the $L1_1$ ordered state ($T/T_c = 0.54$) for the two possible terminations of the alternate variant ((a), (b)) and that of the mixed one (c) corresponding to the (1 1 1) orientation, and for the single mixed variant corresponding to the (1 0 0) orientation (d). The full, dashed and dotted lines represent respectively the concentrations c_0, c_1 and c_2. In figure ((a), (b)) the thin lines illustrate the variation of the two bulk sublattice (α, β) concentrations required to account for $L1_1$ ordering (see Fig. 2).

equilibrium profile is obtained, characterized by two regimes. For $c < 0.5$, there is a strong Cu-enrichment in the surface plane, followed by a Cu-depletion in the first underlayer. If we consider the occupancy of the two sublattices per (1 0 0) plane used to describe the $L1_1$ structure, we observe that long-range order (LRO) is present in the first planes, even in the bulk disordered state ($c < 0.14$). More precisely in the flat part of the isotherm around $c_0 = 0.5$, the LRO parameter in the surface plane, defined as the difference of occupancy between the two sublattices in this plane, is very similar to the bulk one for the equiatomic compound. For $c > 0.5$, the segregation isotherm corresponds to an ideal termination slightly enriched in Cu. This is rather similar to the one obtained for the mixed (1 1 1) variant in its domain of metastability ($c < 0.55$).

Finally, let us note that the existence of a single plateau around equiconcentration is directly related to our (V_1, V_2) parametrization which is unable to account for the existence of the $L1_2$ in bulk phase diagram ($c = 0.25$). This would require to use $V_1 > V_2$, in which case one would also observe an extra plateau corresponding to the surface compound $CuPt_3$ ($c_0 = 0.25$), which is directly linked to the additional presence of the stoichiometric bulk compound $CuPt_3$.

To summarize, these examples have put in evidence the following trends. For an alternate stacking, several terminations are expected, the stablest one being the most enriched by the segregating element in the disordered state. Segregation favours the formation of stoichiometric superficial compounds up to a given depth for off-stoichiometric bulk compound, leading to flat parts on the isotherm. These flat parts begin (or

finish) at stoichiometric bulk compositions. In particular it means that the equilibrium termination of stoichiometric bulk compounds is the ideal one and that small variations of bulk concentration around the stoichiometry can lead to drastic changes for the surface composition. Finally, for a mixed stacking, we generally find only one solution, corresponding to the ideal termination only for stoichiometric compounds. The isotherm should then be formed by a succession of large flat parts corresponding to stoichiometric compositions separated by regions where the surface concentration varies strongly with the bulk concentration. These variations are all the stiffer as the segregation driving forces are higher or the temperature is lower.

5.2. Surface segregation near bulk phase transitions in Cu_cPd_{1-c} system

To illustrate the latter point and to give some examples of the surface behaviour near bulk phase transitions, let us consider the modification of the isotherm as the temperature decreases in the case of the (1 1 1) face for the Cu_cPd_{1-c} system [3,133]. The energetic parameters for this system are given in Table 1 [3]. It can be seen that the Cu-surface segregation driving force is lower than in the Cu–Pt case, the addition of surface energy effect and size effect being almost twice smaller. On the other hand, the value of V_1 being (more commonly) larger than V_2, the phase diagram is now of the Shockley-type [134] with the presence of $L1_2$, L' and $L1_0$ phases at sufficiently low temperatures. The (1 1 1) segregation isotherm for three temperatures: $T/T_c = 1.17$, 0.82 and 0.18 are displayed in Fig. 11.

In the disordered state, one observes near $c = 0.3$ a segregation reversal with respect to the bulk concentration. This is mainly due to the alloying effect, which leads to the segregation of the majority element ($V_1 > 0$). The segregation is not very pronounced due to the competition between the surface energy effect which leads to Cu segregation and the size effect which favours Pd segregation. The weak Cu segregation at $c = 0.5$ is confirmed experimentally [135].

At lower temperature ($T/T_c = 0.82$), the isotherm seems to be not modified: we do not see still the formation of the flat parts corresponding to the stoichiometric surface compounds. However, the concentrations per sublattice in the surface plane are no longer equal (as in the bulk). Moreover, one observes that the average surface concentration is the same on both sides of each two-phases region (D (disorder) - LI_2 and $L1_2$–$L1_0$), whereas the concentrations per sublattice are the same near the $(D - L1_2)$ two-phases region but differ for the $(L1_2 - L1_0)$ one. A detailed study has shown that the $L1_2$ phase is wet in fact by the disordered one [3], leading to a surface induced disorder (SID) [7], whereas the similarity of the average surface concentrations near the $(L1_2 - L1_0)$ two-phases region comes only from an accidental degeneracy.

At $T/T_c = 0.18$, the segregation isotherm drastically changes. It is composed of flat parts for $c_0 = 0$, 0.75 and 1, vertical ones for the stoichiometric bulk concentrations ($c = 0.25$, 0.5 and 0.75) and a region which is characterized by a very weak Cu segregation ($0.25 \leqslant c \leqslant 0.5$), i.e., in which the ideal termination is the equilibrium one. This isotherm presents both the segregation reversal already observed in the high temperature regime near $c = 0.3$ and flat and almost vertical parts similar to those present in Cu–Pt (1 1 1) at low temperature. Due to the change of the nature of the segregant element for $c < 0.3$ the plateau at $c_0 = 0.25$ which could be stabilized (at least for $V_1 > V_2$) in CuPt is replaced by the one at $c_0 = 0$ and the segregation is too weak in the range $0.25 < c < 0.5$ to induce the one at $c_0 = 0.5$. Conversely, due to the lower reduced temperature, plateaus at $c_0 = 0.75$ and 1 are now well formed. It is worth noticing that the vertical parts of the isotherm do not reveal surface phase transitions of the Fowler–Guggenheim type. It can be easily demonstrated since the segregation energy involved in the determination of a given surface sublattice concentration c_0^α only depends on surface concentrations on the other sublattices $c_0^{\omega \neq \alpha}$ and not on c_0^α, see Eq. (24). Thus, the segregation isotherm is found to be of the Langmuir type, i.e., the vertical steps in Fig. 11 correspond only to a very strong, but continuous, increase of c_0^α for a small increase of c^α and not to a discontinuous phase transition.

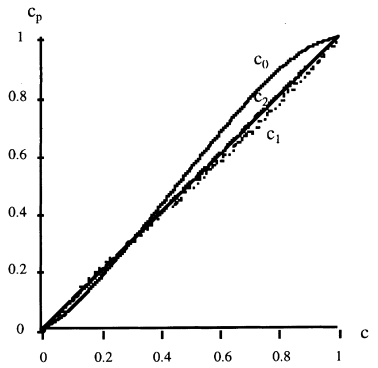

(a)

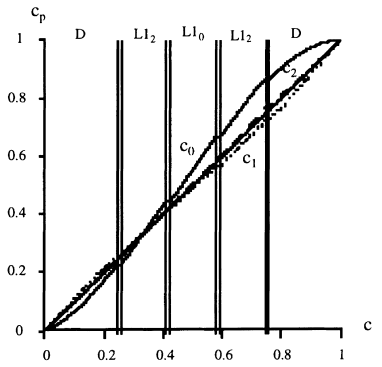

(b)

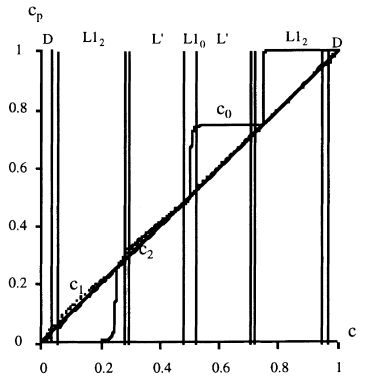

(c)

Fig. 11. Segregation isotherms for the Cu_cPd_{1-c} (1 1 1) system for three different temperatures: $T/T_c = 1.17$ (a), 0.82 (b) and 0.18 (c). The concentrations of the first three layers, c_0, c_1 and c_2, are plotted as a function of the bulk concentration c. The boundaries between the different bulk phases are also indicated.

An other interesting point concerns the variation of the surface concentration as a function of the temperature, in particular for stoichiometric compounds. Indeed, it drastically differs from the usual monotonous behaviour followed by simple Langmuir or Fowler–Guggenheim isotherms. Actually, for concentrations close to those of the stoichiometric compounds, the ideal termination is found to be the equilibrium one at very low and very high temperature but not in an intermediate range. This leads to an unusual enhancement of surface segregation with increasing temperature, whereas a more classical monotonous decrease of segregation with temperature is observed in the other cases [3,133].

5.3. Role of 2-D compounds in surface segregation in Sn_cPt_{1-c} system

Up to now, only the occurrence of a surface ordering with a symmetry similar to one of the bulk ordered phases has been considered, even though it is experimentally known that a new symmetry, specific to the surface plane, could appear. Thus, for the (1 1 1) face of Pt_3Sn compound of $L1_2$ symmetry, a high temperature annealing (1000 K) leads to the observation of a $p(2\times 2)$ structure corresponding to the ideal termination ($c_0 = 0.25$) [136,137]. Then, when the selvedge Sn concentration is lowered by ion bombardment, this structure is replaced by a $(\sqrt{3}\times\sqrt{3})R30^\circ$ one ($c_0 = 0.33$), which is stable up to annealing at $T = 1000$ K [138]. At this temperature, bulk diffusion restores the stoichiometric concentration in the selvedge region and consequently the $p(2\times 2)$ superstructure. As the $(\sqrt{3}\times\sqrt{3})R30^\circ$ symmetry does not occur in (1 1 1) planes in the bulk ordered phases, it is really specific of a surface phenomenon.

The part of the segregation isotherm at $T = 1000$ K ($T/T_c = 0.22$) corresponding to this concentration range is shown in Fig. 12 [3,139]. Surface energy and size effects, which lead to Sn segregation, are about eight times larger than in Cu–Pt, whereas V_1 is almost three times larger than the Cu–Pd one. In addition to the expected plateau at $c_0 = 0.25$, the main characteristics of this isotherm is the additional flat part near $c_0 = 0.33$ corresponding to the stability of the $(\sqrt{3}\times\sqrt{3})R30^\circ$ superstructure, both in the solid solution and in the $L1_2$ bulk phase.

The $(\sqrt{3}\times\sqrt{3})R30^\circ$ superstructure is really 2-D, the c_1 value being very weak and the second underlayer having already both the concentration and the symmetry of the bulk phase (disordered or $L1_2$). Let us remark that the first order phase transition between the $(\sqrt{3}\times\sqrt{3})R30^\circ$ and the $p(2\times 2)$ superstructures for $c = 0.2$ leads to a decrease of the surface concentration whereas the bulk concentration increases! This is in remarkable agreement with the experiments quoted above. The competition between these two superstructures has been studied in the solid solution range by Teraoka [11], showing that the stability of the $(\sqrt{3}\times\sqrt{3})R30^\circ$ surface phase requires a ratio R larger than 1, R being defined as

$$R = -\frac{\Delta h_0 + \Delta E_0^{\text{size}}}{3V}. \tag{41}$$

Consistently this critical value is reached for Pt–Sn, but not for Cu–Pt and Cu–Pd. Experimentally the $(\sqrt{3}\times\sqrt{3})R30^\circ$ superstructure has indeed been observed in systems with bulk ordering tendency and large surface segregation driving forces, such as Cu–Al [140], Cu–Sn [141] and Cu–Sb [142].

6. Coupling between segregation and reconstruction

Let us recall that in the above examples the atomic relaxation has only been taken into account by means of the size effect calculation limited to the impurity case. However, for strong size-mismatch and strong surface enrichment, one could expect some important atomic rearrangements, which will be detailed in the following.

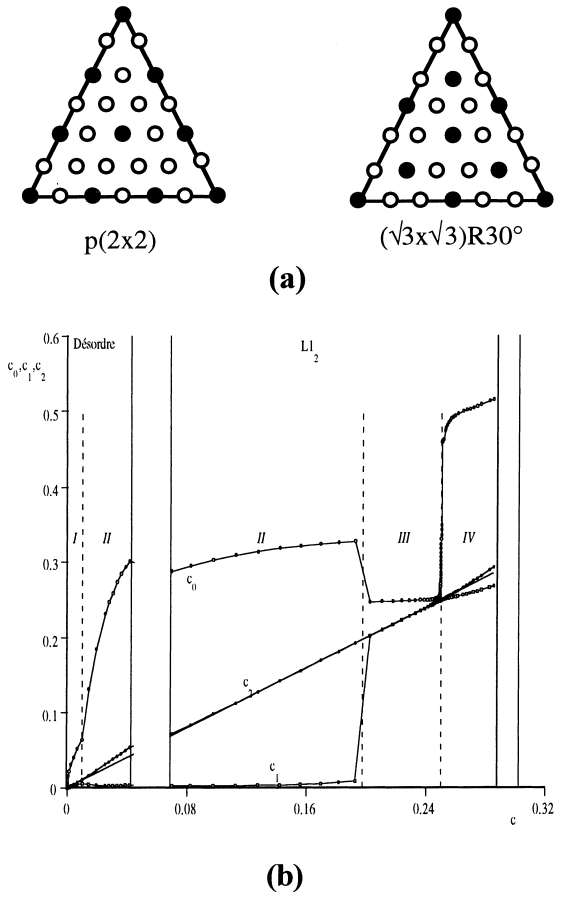

Fig. 12. (a) Possible ordered structures for fcc (1 1 1) layers. (b) Segregation isotherm for $Pt_{1-c}Sn_c$ (1 1 1) at $T/T_c = 0.22$. The stability domains of the different bulk (disorder and $L1_2$) and surface (I = disorder, II = $(\sqrt{3} \times \sqrt{3})R30°$, III = $p(2 \times 2)$ and IV = $L1_0$) phases are separated by vertical lines.

6.1. Size effect (SMILE)

Up to now we have been able to model the size effect only in the case where both surface and bulk are dilute with respect to the impurity. As a consequence, ΔE_0^{size} does not depend on surface concentration so that one will miss its possible saturation with c_0 if it exists. This is probably incorrect when the size-mismatch is large (>10%) and when surface segregation is sufficiently strong to lead to a surface almost pure in the minority element. Indeed, naively speaking, one can imagine that an impurity with a larger atomic radius than the matrix one is less compressed at the surface than in the bulk but that its situation becomes less and less favourable when its concentration increases at the surface. This could even change the sign of ΔE_0^{size} when c_0 is varied beyond a critical surface concentration. These arguments apply to the Cu(Ag) system. It is then essential to account for this possible c_0 dependence of ΔE_0^{size}. This can be done by extending to the case of a finite surface Ag concentration the atomistic treatment previously developed for a single impurity. This has been performed for the (1 1 1) surface [128]. The resulting c_0 dependence of $\Delta E_0^{\text{size}}$is not trivial. As expected, $|\Delta E_0^{\text{size}}|$ decreases monotonously up to a surface concentration $c_0^{\ell} \simeq 0.4$. Beyond this concentration, the simulation shows spontaneous jumps of Ag atoms from the surface towards

adatom positions. These limited expulsions, which occur when the stress reaches a critical value, reflect the difficult coexistence between "big" and "small" atoms at the surface. In fact, this *size-mismatch induced limited expulsion* (SMILE) effect allows the remaining Ag surface atoms to reconstruct towards a local superstructure. When the Ag surface concentration is increased, more and more adatoms are expelled from the surface, leading at completion to a full (10×10) superstructure [62].

In view of these results, one has to revisit the theoretical isotherm of Cu(Ag). Introducing this c_0 dependence of the size effect in the mean-field TBIM equations, within the area preserving map technique, drastically modifies the first layering transition in the segregation process. Indeed, as can be seen in Fig. 13, this transition is now found partial (from a quasi-pure Cu surface to a mixed Cu–Ag one) and asymmetric with respect to $c_0 = 0.5$ [128]. Let us note that such an asymmetry, which comes from the nonlinearity of the c_0-dependence of the size effect, cannot be predicted by usual models. Moreover, the experiments performed on this system compare fairly well with our theoretical predictions, both concerning the partial

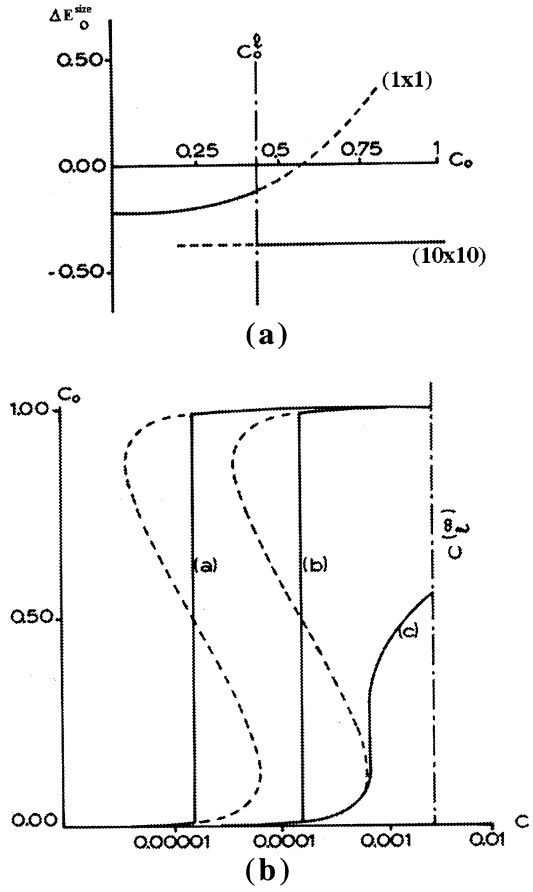

Fig. 13. (a) Surface concentration (c_0) dependence of the size-mismatch energy ΔE_0^{size} in the dilute bulk concentration limit ($c \to 0$) for a Ag_cCu_{1-c} (1 1 1) surface presenting either a (1×1) or (10×10) structure. The solid line is for the stable structure, whereas the dashed line is for the metastable one, the transition occuring at c_0^ℓ. (b) Segregation isotherm (c_0 as a function of c) for Ag_cCu_{1-c} (1 1 1) at $T = 750$ K, calculated using, on one hand a c_0-dependent size-mismatch energy corresponding to either the (10×10) (a) or the (1×1) (c) curve as displayed above, and on the other hand (b) the usual c_0-independent size mismatch as in Fig. 9. $c_\ell^{(\infty)}$ is the bulk solubility limit at this temperature.

and asymmetric character of this layering transition, and the existence of a $(n \times n)$ superstructure which will be discussed hereafter [131,132].

6.2. Influence of surface reconstructions

6.2.1. Tendency to phase separation ($V < 0$)

As mentioned just above, for $V < 0$ and a strong segregation of the A element at the surface of a dilute B(A) alloy, one can expect reconstructions of the surface plane when the size-mismatch is large. The corresponding superstructures can be found by using molecular dynamics simulations with SMA potentials.

Let us illustrate this once again for the Cu(Ag) (1 1 1) system, which can be considered as a model one concerning the atomic structure of one segregated monolayer on a substrate in the case of strong size-mismatch. In that case, LEED-SXRD data reveal the existence of a (9.45×9.45) superstructure while STM images indicate a strong corrugation of the Ag adlayer [143]. Depending on the temperature it appears either as a Moiré structure (low temperature) or as a triangular shaped one (high temperature) [144]. In order to determine theoretically what is the structure which accommodates the most efficiently the size-mismatch, one has not only to optimize the periodicity n of the $(n \times n)$ superstructure, but also to take into account different additional mechanisms (Ag and Cu vacancy formation, partial dislocation loop) to relax the interfacial stress. As a result, the stablest structure is indeed of the $(n \times n)$ type, with $n = 9$ or 10 [62,145]. In addition, one finds two structures which minimize the energy [145,146]. The metastable one corresponds to a quasi-pure Ag(1 1 1) layer on top of a Cu(1 1 1) one, inducing a strong corrugation of the adlayer but also of the Cu substrate, and can be compared to the Moiré structure [62]. The stablest structure is obtained by the formation of partial dislocation loops in the first Cu substrate layer, requiring the formation of four or five Cu vacancies per unit cell in this plane. This efficient relaxation mechanism leads to a strong damping of the corrugation in the Cu underlayers and to a calculated surface morphology in good agreement with the STM images [143,146].

This reconstruction, induced by the Ag segregated layer, leads to the existence of local pressure variations in the first underlayer. It is tempting to think that the big Ag atoms will decorate the tensile sites and conversely will avoid the compressive ones [147]. This could induce drastic modifications concerning segregation in this first underlayer with respect to the previous rigid lattice calculation. To rationalize this effect, we can calculate the segregation energy on each site of the first underlayer, using quenched molecular dynamics simulation within the SMA potential. This leads to the segregation maps shown in Fig. 14. Let us discuss the consequence on the concentration profile for very dilute Cu(Ag) alloys. Since the first layering transition leads to a pure Ag surface with the (10×10) structure, the concentration profile must be affected by the distribution of segregation energies within the first underlayer. For the Moiré structure, the segregation map presents on this layer both favourable and unfavourable sites for Ag segregation ($0.3\ \text{eV} > \Delta E_1 > -0.4\ \text{eV}$). Therefore, the resulting chemical structure will be of pyramidal type, the Ag atoms decorating the tensile pyramidal-shaped regions of the first layers [147]. This probably forbids the second layering transition expected from rigid lattice calculations [127–130]. For the structure stabilized by the formation of partial dislocation loops, the segregation map on the first underlayer is drastically different, since one recovers a tendency to Ag segregation on all sites ($-0.1\ \text{eV} > \Delta E_1 > -0.4\ \text{eV}$). As a consequence, a second layering transition remains plausible in this structure.

6.2.2. Tendency to bulk ordering ($V > 0$)

(a) *Influence of reconstructions*: A large amount of experiments have been performed on Pt–M alloys with M = (Fe, Co, Ni) [29]. If all these alloys have a large tendency to order, they have an other characteristic feature. They are composed by one metal (Pt) for which the (1 0 0) and (110) surfaces reconstruct [148], whereas the same surfaces do not reconstruct for the M-constituent. Then one can ask on the existence of a

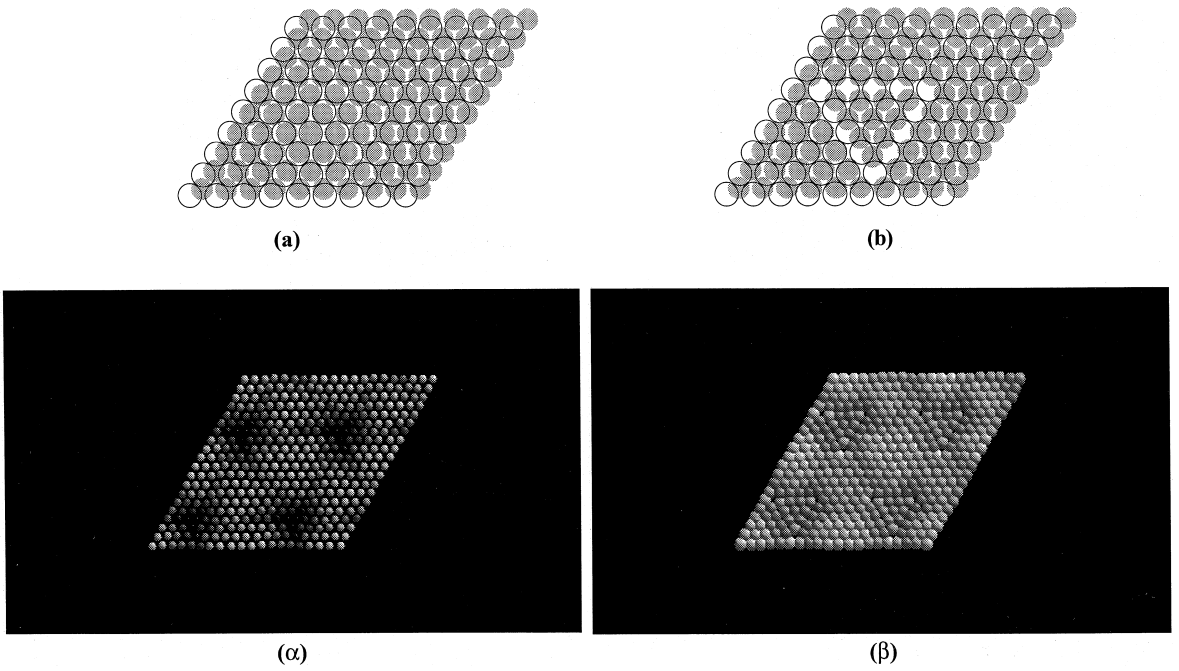

Fig. 14. *Upper part*: schematical top view of the stacking fault which allows to avoid unfavourable on-top positions (left-hand side) in one Ag/Cu (1 1 1) $p(10 \times 10)$ unit cell, by introduction of a partial dislocation loop (right hand side). Only the first two layers are shown before relaxation, the Ag(Cu) atoms being represented by empty (grey) circles. *Lower part*: segregation energy map of the first Cu underlayer after relaxation for four unit cells of the type described above, without (left-hand side) and with (right-hand side) the dislocation loop. The grey scale illustrates the segregation energy variation from the most Ag favoured sites (white spheres: $\Delta E_1^{\min} = -0.4$ eV/at) up to the less favoured ones (black spheres: $\Delta E_1^{\max} = +0.3$ eV/atom).

critical concentration c_c in the alloys Pt_cM_{1-c} beyond which surface reconstruction should occur. Moreover, the alloy surface reconstruction can differ from the pure metal (Pt) one; in particular it can evolve with the surface (or bulk) concentration. In a first time, we will discuss the coupling between segregation and reconstruction for the (1 0 0) face before considering the (1 1 0) one.

The reconstruction of the (1 0 0) face of Pt (as for Ir and Au) can be interpreted in terms of quasi-hexagonal unit cells. The surface energy is minimized by increasing the atomic density and adopting a fcc (1 1 1)-like structure. The quasi-hexagonal (5×1) unit can be obtained from the unreconstructed structure by shifting one $\langle 0\ 1\ 1 \rangle$ row over two along the $\langle 0\ 1\ 1 \rangle$ direction and by adding an homogeneous compression along the $\langle 0\ \bar{1}\ 1 \rangle$ [148]. From STM and LEED studies of Pt_cM_{1-c} (1 0 0), it appears that shifted rows occur for low value of c, but without long range order between them [149–151]. These displacements allow to relax the stress induced by the segregating big atoms (Pt) and can be viewed as a precursor of the pseudohexagonal reconstruction of Pt (1 0 0). Increasing the Pt concentration leads to $(n \times 1)$ superstructures which can be decomposed into (5×1) domains separated by shifted rows. The transition between the reconstructed structure and the unreconstructed one is found to be between $c = 0.25$ and $c = 0.5$ in Pt_cNi_{1-c} [149,150] and lower than 0.25 in Pt_cCo_{1-c} [151,152]. An interesting consequence of this coupling between segregation and reconstruction concerns the nature of the concentration profile. As the $\langle 0\ 1\ 1 \rangle$ rows are not crystallographically equivalent in the $(n \times 1)$ reconstruction, the local pressure varies from one to the other. As a consequence, there is a concentration specific for each $\langle 0\ 1\ 1 \rangle$ row at the surface and in the first underlayers. It means that the structural reconstruction induces long range order in the first surface planes. It is then not surprising that the average concentration per plane

does not follow the oscillatory behaviour predicted in the disordered state for the alloy characterized by $V > 0$.

The (1 1 0) face in PtM alloys has been studied for $Pt_{80}Fe_{20}$ in the bulk ordered state [153,154] and for $Pt_{25}Co_{75}$ and $Pt_{35}Co_{65}$ in the disordered state [151,152]. The behaviour drastically differs between the two systems. For $Pt_{80}Fe_{20}$, the (1 1 0) face reconstructs as in pure Pt with the (2×1) and (3×1) missing-row reconstructions. This is correlated with the stability of the pure Pt termination in this ordered alloy. At the opposite, in Pt–Co alloys, the surface plane is unreconstructed and largely depleted in Pt. (2×1) superstructure can be obtained, but it comes now from chemical order in the first underlayer. Thus, additional experiments would be very useful to discriminate the role of the bulk ordering from the one of the bulk concentration in the stability of the reconstruction for the (1 1 0) face.

From these examples, we can conclude that the coupling between segregation and structural reconstruction leads to a large variety of phenomena, which remain to be explored both experimentally and theoretically.

(b) *Steps*: For $V > 0$, another competition between chemical and geometrical order can occur in presence of steps at the surface. Indeed, when considering a bulk ordered state corresponding to an alternate stacking of pure planes, $\{\ldots/A/B/A/B/\ldots\}$, the ideal termination of a vicinal surface with single steps will present simultaneously stable and metastable (or unstable) terminations. Then, depending on the relative importance of alloying effect and surface local fields on one hand and on the energy difference between single and double steps on the other hand, the surface could present either single steps and some unfavourable terminations or double steps and then a single favourable termination [95]! This problem does not arise at high temperature since the alternate stacking disappears in the disordered state. Indeed, a transition from double steps to single steps, associated to the bulk order–disorder transition, has been experimentally evidenced in Cu–Pd [32].

7. Conclusion and perspectives

From what has been described above, it appears that the old problem of surface segregation can now be tackled with modern theoretical tools, allowing us (in most cases) to answer the more and more subtle questions raised by experiments which give now access to a quasi microscopic view of the phenomenon. This is essentially due to the development of efficient statistical methods, grounded on interatomic potentials derived from the electronic structure. Eventhough the first success of these methods has been to justify the "old" empirical rules explaining surface segregation in terms of three simple driving forces (difference in surface energies and atomic radii between the two components and tendency for them to mix or phase separate in the bulk), they also have set the limits of these rules, and given tools to go beyond (proper treatment of the size effect, surface enhancement of the alloying term, exhaustive treatment of the multisolution character of the problem). Moreover, they have evidenced a whole (rich) class of phenomena occurring close to bulk phase transitions, in which case the surface seems to play a precursor role by means of specific surface transitions (pre-phase separation or pre-phase ordering). Finally, it is now possible to account for the influence of lattice relaxations on chemical ordering at the surface.

Anyway some points remain unclear in surface segregation modelling, which would require more investigation. The first one concerns the electronic structure of alloy surfaces and the link between semi-empirical approaches such as the ones developed here and the ab initio calculations, which are the topics of other contributions to that book (Ruban–Skriver, Drchal et al.). The second point deals with the statistical methods used to determine the thermodynamical equilibrium state of these surfaces, and in particular Monte Carlo simulations which should include both crystallographic (reconstructions) and morphological (steps, roughness) possible rearrangements. Such a mixed treatment is indeed necessary if one aims at comparing segregation at surfaces and at grain boundaries. It is also required when studying segregation in

finite systems such as bimetallic clusters (which means calculating their phase diagrams). In an other context, it would be interesting to relate surface segregation in binary systems with that in ternary ones, including both actual ternary alloys (cosegregation, see the contribution by Wynblatt–Landa) or effective ones resulting from the segregation of bulk interstitial species into the surface layer or above. Finally, let us mention that there exists a close connection between equilibrium segregation at alloy surfaces and dissolution kinetics of deposited layers into a substrate, leading to the formation of metastable surface alloys, which are widely studied at the moment and are mentioned in the contributions of Wille–Dreysse and Ferrante.

Acknowledgements

The authors are very grateful to the following persons for very useful and nice discussions on various aspects of segregation problems: Bernard Aufray, Fabienne Berthier, Stéphanie Delage, Jérôme Eugène, Jean-Marc Gay, Jacek Goniakowski, Abdelali Khoutami, Philippe Maugain, Jean-Marc Roussel, Samir Sawaya, Frédéric Soisson and Paul Wynblatt.

References

[1] J.W. Gibbs, The Collected Works of J.W. Gibbs, vol. 1, Yale University Press, New Haven, 1948.
[2] J.M. Blakely, H.V. Thapliyal, Interfacial Segregation, In: W.C. Johnson, J.M. Blakely (Eds.), AMS, Metals Park, OH, 1979, p. 137.
[3] C. Gallis, Thèse Université Paris VI, 1997.
[4] P. Wynblatt, R.C. Ku, Interfacial Segregation, in: W.C. Johnson, J.M. Blakely (Eds.), AMS, Metals Park, OH, 1979, p. 115.
[5] F.L. Williams, D. Nason, Surf. Sci. 45 (1974) 377.
[6] J. Tersoff, Phys. Rev. B 42 (1990) 10965.
[7] R. Lipowsky, Critical Phenomena at Surfaces and Interfaces, Springer Tracts in Modern Physics, Springer, Berlin, 1993, p. 127.
[8] W. Schweika, K. Binder, D.P. Landau, Phys. Rev. Lett. 65 (1990) 3321.
[9] R. Lipowsky, Phys. Rev. Lett. 49 (1982) 1575.
[10] Y. Teraoka, T. Seto, Surf. Sci. 255 (1991) 209.
[11] Y. Teraoka, Surf. Sci. 235 (1990) 249.
[12] K. Binder, D.P. Landau, Phys. Rev. Lett. 52 (1984) 318.
[13] K.H. Rieder, Dynamical phenomena at surfaces, interfaces and superlattices, Springer Series in Surface Sciences, vol. 3, Berlin, 1985.
[14] C.B. Duke, Surf. Sci. 299/300 (1994) 24.
[15] D. Dufayard, R. Baudoing, Y. Gauthiere, Surf. Sci. 233 (1990) 223.
[16] C.J. Powell, Surf. Sci. 299/300 (1994) 34.
[17] D.P. Woodruff, Surf. Sci. 299/300 (1994) 183.
[18] F. Jona, J. Phys. C: Solid State Phys. 11 (1978) 4271.
[19] Y. Gauthier, R. Baudoing, In: P.A. Dowben, A. Miller (Eds.), Surface Segregation Phenomena CRC Press, Florida, 1990, p. 169.
[20] J.W. Rabalais, Surf. Sci. 299/300 (1994) 219.
[21] L.C. Feldman, Surf. Sci. 299/300 (1994) 233.
[22] H. Reichert, P.J. Eng, H. Dosch, I.K. Robinson, Phys. Rev. Lett. 74 (1995) 2006.
[23] T.T. Tsong, R. Casanova, Phys. Rev. Lett. 47 (1981) 113.
[24] T.T. Tsong, Surf. Sci. 299/300 (1994) 153.
[25] H. Rohrer, Surf. Sci. 299/300 (1994) 956.
[26] M. Schmid, H. Stadler, P. Varga, Phys. Rev. Lett. 70 (1993) 1441.
[27] C. Cohen, A. L'Hoir, J. Moulin, D. Schmaus, M. Sotto, J.-L. Domange, J.-C. Bouillard, Surf. Sci. 339 (1995) 41.
[28] D. Sondericker, F. Jona, P.M. Marcus, Phys. Rev. B 33 (1986) 900.
[29] Y. Gauthier, Surf. Rev. Lett. 3 (1996) 1663.
[30] P. Varga, M. Schmid, W. Hofer, Surf. Rev. Lett. 3 (1996) 1831.
[31] P.T. Wouda, B.E. Nieuwenhuys, M. Schmid, P. Varga, Surf. Sci. 359 (1996) 17.

[32] L. Barbier, B. Salanon, A. Loiseau, Phys. Rev. B 50 (1994) 4929.
[33] M.C. Desjonquères, D. Spanjaard, Phys. Rev. B 35 (1987) 952.
[34] J.P. Muscat, J. Phys. C 15 (1982) 867.
[35] K. Masuda-Jindo, Phys. Lett. A 107 (1985) 185.
[36] R. Riedinger, H. Dreyssé, Phys. Rev. B 27 (1983) 2073.
[37] H. Dreyssé, R. Riedinger, Phys. Rev. B 28 (1983) 5669.
[38] M. Alden, H.L. Skriver, B. Johansson, Phys. Rev. Lett. 71 (1993) 2449.
[39] F. Ducastelle, J. Phys. Paris 31 (1970) 1055.
[40] R. Haydock, Solid State Phys. 35 (1980) 216.
[41] P. Turchi, F. Ducastelle, G. Tréglia, J. Phys. C: Solid State Phys. 15 (1982) 2891.
[42] G. Allan, M. Lannoo, Phys. Stat. Sol. (b) 74 (1976) 409.
[43] J. Friedel, Nuovo Cimento 7 (1958) 287.
[44] D. Spanjaard, C. Guillot, M.C. Desjonquères, G. Tréglia, J. Lecante, Surf. Sci. Rep. 5 (1985) 1.
[45] B. Johansson, N. Martensson, Phys. Rev. B 21 (1980) 4427.
[46] G.N. Derry, Surf. Sci. 316 (1994) L1044.
[47] M. Said, M.C. Desjonquères, D. Spanjaard, Surf. Sci. 287/288 (1993) 780.
[48] J.D. Eshelby, Adv. Sol. State Phys. 3 (1956) 79.
[49] J. Friedel, Adv. Phys. 3 (1954) 446.
[50] P. Wynblatt, R.C. Ku, Surf. Sci. 65 (1977) 511.
[51] S.M. Foiles, in: P.A. Dowben, A. Miller (Eds.), Surface Segregation Phenomena, CRC Press, Florida, 1990, p. 79.
[52] M.W. Finnis, J.E. Sinclair, Phil. Mag. B 50 (1984) 45.
[53] V. Rosato, M. Guillopé, B. Legrand, Phil. Mag. A 59 (1989) 321.
[54] J.K. Norskov, Phys. Rev. B 26 (1982) 2875.
[55] K.W. Jacobsen, J.K. Norskov, M.J. Puska, Phys. Rev. B 35 (1987) 7423.
[56] G. Tréglia, B. Legrand, F. Ducastelle, Europhys. Lett. 7 (1988) 575.
[57] D. Hersant, Thèse Université Paris XI, 1991.
[58] J.H. Rose, J. Ferrante, J.R. Smith, Phys. Rev. Lett. 47 (1981) 675.
[59] J.H. Rose, J.R. Smith, F. Guinea, J. Ferrante, Phys. Rev. B 29 (1984) 2963.
[60] D. Spanjaard, M.C. Desjonquères, Phys. Rev. B 30 (1984) 4822.
[61] A. Banerjea, J.R. Smith, Phys. Rev. B 37 (1988) 6632.
[62] C. Mottet, G. Tréglia, B. Legrand, Phys. Rev. B 46 (1992) 16018.
[63] M.S. Daw, M.I. Baskes, Phys. Rev. Lett. 50 (1983) 1285.
[64] M.S. Daw, M.I. Baskes, Phys. Rev. B 29 (1984) 6443.
[65] F. Ercolessi, E. Tosatti, M. Parrinello, Phys. Rev. Lett. 57 (1986) 719.
[66] F. Ercolessi, M. Parrinello, E. Tosatti, Philos. Mag. A 58 (1988) 213.
[67] M. Nastar, Thèse Université Paris VI, 1994.
[68] J. Sokolov, F. Jona, P.M. Marcus, Solid State Commun. 49 (1984) 307.
[69] G. Allan, M. Lannoo, Surf. Sci. 40 (1973) 375.
[70] R.P. Gupta, Phys. Rev. B 23 (1981) 6265.
[71] J. Sokolov, F. Jona, P.M. Marcus, J. Phys. C 17 (1984) 371.
[72] J.S. Luo, B. Legrand, Phys. Rev. B 38 (1988) 1728.
[73] M. Guillopé, B. Legrand, Surf. Sci. 215 (1989) 577.
[74] N.T. Barrett, C. Guillot, B. Villette, G. Tréglia, B. Legrand, Surf. Sci. 251/252 (1991) 717.
[75] P.E.A. Turchi, Thèse Université Paris VI, 1984.
[76] F. Ducastelle, Order and Phase Stability in Alloys, North Holland, 1991.
[77] F. Ducastelle, F. Gautier, J. Phys. F 6 (1976) 2039.
[78] B. Velicky, S. Kirkpatrick, H. Ehrenreich, Phys. Rev. 175 (1968) 747.
[79] F. Ducastelle, B. Legrand, G. Tréglia, Prog. of Theoretical Physics, suppl 101 (1990) 159.
[80] A. Bieber, F. Gautier, G. Tréglia, F. Ducastelle, Solid State Commun. 39 (1981) 149.
[81] D. Tomanek, A.A. Aligia, C.A. Balseiro, Phys. Rev. B 32 (1985) 5051.
[82] G. Tréglia, B. Legrand, Phys. Rev. B 35 (1987) 4338.
[83] F.F. Abraham, N.H. Tsai, G.M. Pound, Surf. Sci. 83 (1979) 406.
[84] F.F. Abraham, C.R. Brundle, J. Vac. Sci. Technol. 18 (1981) 506.
[85] C. Mottet, Thèse Université Aix-Marseille II, 1997.
[86] F. Berthier, B. Legrand, G. Tréglia, Acta Mater., (submitted).
[87] I. Meunier, G. Tréglia, B. Legrand, Surf. Sci., (submitted).
[88] S. Sawaya, J. Goniakowski, C. Mottet, A. Saúl, G. Tréglia, Phys. Rev. B 56 (1988) 12161.

[89] A.P. Sutton, M.W. Finnis, D.G. Pettifor, Y. Ohta, J. Phys. C 21 (1988) 35.
[90] B. Legrand, G. Tréglia, Surf. Sci. 236 (1990) 398.
[91] A. Sakai, T. Sakurai, Surf. Sci. 138 (1984) 159.
[92] R. Pandit, M. Wortis, Phys. Rev. B 25 (1982) 3226.
[93] G. Tréglia, B. Legrand, P. Maugain, Surf. Sci. 225 (1990) 319.
[94] A. Senhaji, G. Tréglia, B. Legrand, Surf. Sci. 307–309 (1994) 440.
[95] A. Senhaji, Thèse Université Paris XI, 1993.
[96] B. Legrand, G. Tréglia, F. Ducastelle, Phys. Rev. B 41 (1990) 4422.
[97] M.H. Jensen, P. Bak, Phys. Rev. B 27 (1983) 6853.
[98] A. Senhaji, G. Tréglia, B. Legrand, N.T. Barrett, C. Guillot, B. Villette, Surf. Sci. 274 (1992) 297.
[99] N. Metropolis, A.W. Metropolis, M.N. Rosenbluth, A.H. Teller, E. Teller, J. Chem. Phys. 21 (1953) 1087.
[100] S.M. Foiles, Phys. Rev. B 32 (1985) 7685.
[101] R. Tétot, B. Legrand, J. Creuze, F. Berthier, (to be published).
[102] J.D. Rittner, S.M. Foiles, D.N. Seidman, Phys. Rev. B 50 (1994) 12004.
[103] R. Kikuchi, Phys. Rev. 81 (1951) 988.
[104] V. Kumar, K.H. Bennemann, Phys. Rev. Lett. 53 (1984) 278.
[105] J.M. Sanchez, J.L. Moran-Lopez, Surf. Sci. 157 (1985) L297.
[106] Y. Teraoka, Surf. Sci. 232 (1990) 193.
[107] Y. Teraoka, Surf. Sci. 233 (1990) L97.
[108] T.C. Lubensky, M.H. Rubin, Phys. Rev. B 12 (1975) 3885.
[109] E.H. Hauge, Phys. Rev. B 33 (1986) 3322.
[110] R. Lipowsky, Ferroelectrics 73 (1987) 69.
[111] J.L. Moran-Lopez, F. Mejia-Lira, K.H. Bennemann, Phys. Rev. Lett. 54 (1985) 1936.
[112] F. Mejia-Lira, K.H. Bennemann, J.L. Moran-Lopez, Phys. Rev. B 32 (1985) 5925.
[113] D.M. Kroll, G. Gompper, Phys. Rev. B 36 (1987) 7078.
[114] R. Najafabadi, H.Y. Wang, D.J. Srolovitz, R. LeSar, Acta metall. mater. 39 (1991) 3071.
[115] H.Y. Wang, R. Najafabadi, D.J. Srolovitz, R. LeSar, Phys. Rev. B 45 (1992) 12028.
[116] H.Y. Wang, R. Najafabadi, D.J. Srolovitz, R. LeSar, Acta Metall. Mater. 41 (1993) 2533.
[117] A. Saúl, G. Tréglia, B. Legrand, Note Technique SRMP 94.62 (1994) 83.
[118] Y. Gauthier, Y. Joly, R. Baudoing, J. Rundgren, Phys. Rev. B 31 (1985) 6216.
[119] Y. Gauthier, R. Baudoing, M. Lundberg, J. Rundgren, Phys. Rev. B 35 (1987) 7867.
[120] W. Hofer, X. Fresenius, J. Anal. Chem. 346 (1993) 246.
[121] Y. Gauthier, R. Baudoing, J. Jupille, Phys. Rev. B 40 (1989) 1500.
[122] A. Khoutami, B. Legrand, G. Tréglia, Surf. Sci. 287/288 (1993) 851.
[123] J.F. Van der Veen, B. Pluis, A.G. Denier van der Gon, in: M.G. Lagally (Ed.), Kinetics of Ordering and Growth at Surfaces, Plenum Press, New York, 1990, p. 343.
[124] Y. Liu, P. Wynblatt, Surf. Sci. 240 (1990) 245.
[125] Y. Liu, P. Wynblatt, Surf. Sci. 241 (1991) L21.
[126] Y. Liu, P. Wynblatt, Surf. Sci. 290 (1993) 335.
[127] J. Eugène, G. Tréglia, B. Legrand, B. Aufray, F. Cabané, Surf. Sci. 251/252 (1991) 664.
[128] G. Tréglia, B. Legrand, J. Eugène, B. Aufray, F. Cabané, Phys. Rev. B 44 (1991) 5842.
[129] A. Saúl, B. Legrand, G. Tréglia, Phys. Rev. B 50 (1994) 1912.
[130] A. Saúl, B. Legrand, G. Tréglia, Surf. Sci. 331–333 (1995) 805.
[131] J. Eugène, B. Aufray, F. Cabané, Surf. Sci. 241 (1991) 1.
[132] Y. Liu, P. Wynblatt, Surf. Sci. 310 (1994) 27.
[133] C. Gallis, B. Legrand, A. Saúl, G. Tréglia, P. Hecquet, B. Salanon, Surf. Sci. 352–354 (1996) 588.
[134] W. Shockley, J. Chem. Phys. 6 (1938) 130.
[135] A. Rochefort, M. Abon, P. Delichère, J.C. Bertolini, Surf. Sci. 294 (1993) 43.
[136] A. Atrei, U. Bardi, G. Rovida, M. Torrini, E. Zanazzi, P.N. Ross, Phys. Rev. B 46 (1992) 1649.
[137] N. Haner, P.N. Ross, U. Bardi, Surf. Sci. 249 (1991) 15.
[138] A. Atrei, U. Bardi, M. Torrini, E. Zanazzi, G. Rovida, H. Kasamura, M. Kudo, J. Phys. Condens. Matter 5 (1993) L207.
[139] C. Gallis, B. Legrand, G. Tréglia, Surf. Sci. 377–379 (1997) 1033.
[140] R.J. Baird, D.F. Ogletree, M.A. van Hove, G.A. Somorjai, Surf. Sci. 165 (1986) 345.
[141] J. Erlewein, S. Hofmann, Surf. Sci. 68 (1977) 71.
[142] H. Giordano, B. Aufray, Surf. Sci. 307–309 (1994) 816.
[143] B. Aufray, M. Göthelid, J.-M. Gay, C. Mottet, E. Landemark, G. Falkenberg, L. Lottermoser, L. Seehofer, R.L. Johnson, Microsc. Microanal. Microstruct. 8 (1997) 167.

[144] F. Besenbacher, L. Pleth Nielsen, P.T. Sprunger, in: D.A. King, D.P. Woodruff, (Eds.), The Chemical Physics of Solid Surfaces and Heterogeneous Catalysis, vol. 8, Chapter 10, Elsevier, Amsterdam, 1997.
[145] J. Jacobsen, L. Pleth Nielsen, F. Besenbacher, I. Stensgaard, E. Lægsgaard, T. Rasmussen, K.W. Jacobsen, J.K. Norskov, Phys. Rev. Lett. 75 (1995) 489.
[146] I. Meunier, G. Tréglia, J.-M. Gay, B. Aufray, B. Legrand, Phys. Rev. B 59 (15 April 1999).
[147] C. Mottet, G. Tréglia, B. Legrand, Surf. Sci. 287/288 (1993) 476.
[148] M.A. Van Hove, R. Koestner, P.C. Stair, J.P. Biberian, L.L. Kesmodel, I. Bartos, G.A. Somorjai, Surf. Sci. 103 (1981) 189.
[149] M. Schmid, A. Biedermann, S.D. Böhmig, P. Weigand, P. Varga, Surf. Sci. 318 (1994) 289.
[150] Y. Gauthier, R. Baudoing-Savois, J. Rundgren, M. Hammar, M. Gothelid, Surf. Sci. 327 (1995) 100.
[151] Y. Gauthier, P. Dolle, R. Baudoing-Savois, W. Hebenstreit, E. Platzgummer, M. Schmid, P. Varga, Surf. Sci. 396 (1998) 137.
[152] J.-M. Bugnard, Thèse Université Grenoble I, 1995.
[153] R. Baudoing-Savois, Y. Gauthier, W. Moritz, Phys. Rev. B 44 (1991) 12977.
[154] M. Hammar, Y. Gauthier, M. Göthelid, U.O. Karlsson, S.A. Flodström, A. Rosengren, J. Phys. Condens. Matter 5 (1993) 2837.